Cardiovascular Research (2016) **111**, 105–118
doi:10.1093/cvr/cvw090

# Endothelial lipid phosphate phosphatase-3 deficiency that disrupts the endothelial barrier function is a modifier of cardiovascular development

**Ishita Chatterjee, Jugajyoti Baruah, Erin E. Lurie, and Kishore K. Wary***

Department of Pharmacology, University of Illinois, 835 S. Wolcott Avenue, Room E403, Chicago, IL 60612, USA

*Received 9 November 2015; revised 5 April 2016; accepted 21 April 2016; online publish-ahead-of-print 28 April 2016*

**Time for primary review: 49 days**

**Aims** Lipid phosphate phosphatase-3 (LPP3) is expressed at high levels in endothelial cells (ECs). Although LPP3 is known to hydrolyse the phosphate group from lysolipids such as spingosine-1-phosphate and its structural homologues, the function of *Lpp3* in ECs is not completely understood. In this study, we investigated how tyrosine-protein kinase receptor (*TEK* or *Tie2)* promoter–dependent deletion of *Lpp3* alters EC activities.

**Methods and results** $Lpp3^{fl/fl}$ mice were crossed with the *tg.*$Tie2^{Cre}$ transgenic line. Vasculogenesis occurred normally in embryos with $Tie2^{Cre}$-mediated deletion of *Lpp3* (called $Lpp3^{ECKO}$), but embryonic lethality occurred in two waves, the first wave between E8.5 and E10.5, while the second between E11.5 and E13.5. Lethality in $Lpp3^{ECKO}$ embryos after E11.5 was accompanied by vascular leakage and haemorrhage, which likely resulted in insufficient cardiovascular development. Analyses of haematoxylin- and eosin-stained heart sections from E11.5 $Lpp3^{ECKO}$ embryos showed insufficient heart growth associated with decreased trabeculation, reduced growth of the compact wall, and absence of cardiac cushions. Staining followed by microscopic analyses of $Lpp3^{ECKO}$ embryos revealed the presence of apoptotic ECs. Furthermore, *Lpp3*-deficient ECs showed decreased gene expression and protein levels of *Cyclin-D1*, *VE-cadherin*, *Fibronectin*, *Klf2*, and *Klf4*. To determine the underlying mechanisms of vascular leakage and barrier disruption, we performed knockdown and rescue experiments in cultured ECs. *LPP3* knockdown decreased transendothelial electrical resistance and increased permeability. Re-expression of *β-catenin* cDNA in *LPP3*-knockdown ECs partially restored the effect of the LPP3 loss, whereas re-expression of *p120ctn* cDNA did not.

**Conclusion** These findings demonstrate the essential roles of LPP3 in the maturation of EC barrier integrity and normal cardiovascular development.

**Keywords** Beta-catenin • LPP3 • PPAP2b • VE-cadherin • Neovascularization

## 1. Introduction

Cell-adhesion events mediated by VE-cadherins, catenins, and extracellular matrix (ECM) proteins play decisive roles in the development of vascular endothelial cells (ECs) and the maintenance of the vascular system.[1–6] In this regard, the pivotal roles played by β-catenin and VE-cadherin in the formation of adherens junctions (AJs) during the development and maintenance of blood vessels have been investigated.[1–6] For example, the deletion of *VE-cadherin* (*Cdh5*) was found to inhibit vascular remodelling and induce degradation of vascular integrity, resulting in early embryonic lethality.[3,4] The conditional deletion of the *β-catenin* gene in ECs induces a defective vascular pattern and reduces vascular integrity.[5] Cell adhesion mediated by binding of integrins to ECM proteins such as fibronectin and laminins also plays an equally important role in several aspects of vascular development and differentiation.[1,2] A key role for β-catenin beyond binding to VE-cadherin has been established in the transduction of Wnt signals.[7–10] Canonical Wnt signalling propagates translocation of stabilized β-catenin to the nucleus, where it coactivates the transcription factor T-cell factor/lymphocyte enhancer binding factor (TCF-1/LEF-1).[9,10] In addition, β-catenin also plays a key role in EC and heart valve development and activates transcription factors such as Er71/Etv2, which plays a

* Corresponding author. Tel: +1 312 413 9582; fax: +1 312 996 1225, E-mail: kkwary@uic.edu

key role in the generation of Fetal liver kinase (Flk)1$^{+}$ ECs.[11,12] However, the molecular mechanisms underlying these processes are not clearly understood.

Lipid phosphate phosphatases (LPPs), most recently changed the nomenclature to phospholipid phosphatases (PLPPs), are encoded by phosphatidic acid phosphatases (*PPAP2b*), represent a family of ectoenzymes that are known to cleave the phosphate group from sphingosine-1-phosphate (S1P) and its structural homologues.[13–15] The three major isoforms LPP1, LPP2, and LPP3 are distributed unevenly in the endoplasmic reticulum, cytosol, plasma membrane, and caveolae.[13–17] A more recent study reported the localization of LPP3 to cell–cell contact sites.[18] Previous studies have documented the ability of LPPs to down-regulate cell signalling.[13–17] We previously detected LPP3 in a bioassay for angiogenesis and reported the ability of LPP3 to regulate cell-adhesion events.[19,20] We also showed that anti-LPP3 antibody blocked basic fibroblast growth factor (bFGF)- and vascular endothelial growth factor (VEGF)-mediated angiogenic activities of ECs.[21] In addition, we reported the ability of LPP3 to regulate tumour growth *in vivo*.[21–23]

Conventional deletion of the *Lpp3* gene results in severe embryonic developmental abnormalities such as defective formation of the chorioallantois, placenta, and yolk sac vasculature, suggesting a critical function of Lpp3 in early mouse development.[24] Thus, complete analysis of the *in vivo* function of Lpp3 is hampered by early embryonic lethality.[24] The results obtained on *Mx1*$^{Cre}$- or *Cdh5*$^{CreERT2}$-mediated deletion of *Lpp3* indicated its ability to control the Lpp3–S1P steady state in relation to thymic T-cell egression.[25] Lpp3 deletion altered smooth muscle cell phenotypes[26] and vascular inflammation.[27] These studies described the ability of Lpp3 to act as an enzyme; however, they did not address the behaviour of ECs in relation to cardiovascular development. Therefore, we generated *Lpp3*$^{fl/fl}$ mice and crossed them with the *Tie2*$^{Cre}$ transgenic line; we used these mice to investigate the crucial role played by *Lpp3* in EC barrier integrity and cardiovascular development.

# 2. Methods

## 2.1 Materials and methods

### 2.1.1 Antibodies and reagents

Production, characterization, and use of rabbit anti-LPP3 antibody have been previously described,[19–22] and anti-LPP3 antibodies were used at 1.5 μg/mL concentration. Mouse anti-VCIP/LPP3 (39-1000) monoclonal antibody (mAb) was purchased from Invitrogen (Carlsbad, CA, USA), used at 2.0 μg/mL concentration. Rabbit-anti-LPP2 polyclonal antibody (pAb) was obtained from Exalpha Biologicals, Inc. (Shirley, MA, USA), prepared and used at 2.0 μg/mL. Rabbit anti-Cyclin-D1 (2978) and rabbit anti-cleaved caspase-3 (9664) were bought from Cell Signaling Technology, Inc. (Denvers, MA, USA), and these antibodies prepared and used at 1.25 μg/mL. Mouse anti-β-catenin (SC-7963), anti-VE cadherin (SC-9989 and SC-64586), mouse anti-p120 catenin (SC-23872), anti-DLL4 (SC-28915), mouse anti-p53 (SC-6243), and mouse anti-p21 (SC-397) antibodies were purchased from Santa Cruz Biotechnology (Santa Cruz, CA, USA), and these antibodies were used at 1.5 μg/mL concentrations. Rabbit anti-LPP1 (AV42146), rabbit-anti-β-catenin (C7738 and C2206), and anti-Fibronectin were purchased from Sigma (St. Louis, MO, USA), and these antibodies were prepared and used at 1.75 μg/mL concentration. Rat anti-Flk1 (Avas12a1) mAb was purchased from Novus Biologicals (Littleton, CO, USA), used at a concentration of 2.0 μg/mL. Rabbit anti-vWF (AB7356), anti-Cre (69050-3), and thrombin (605206) were purchased from EMD-Millipore (Billerica, MA, USA), and anti-vWF and anti-Cre antibodies were prepared and used at 1.25 μg/mL concentrations. Secondary antibodies were purchased from Promega Corp. (Madison, WI, USA) or from KPL Inc. (Gaithersburg, MD, USA). Growth factor-reduced Matrigel and rat anti-PECAM-1 (CD31) antibody (550274) were bought from BD Bioscience (Franklin Lakes, NJ, USA). Vaso-TACS *in situ* apoptosis detection kit (4826-30-K) was purchased from Trevigen (Gaithersburg, MD, USA). Substrates and alkaline phosphatase for histological experiments were purchased from Vector Labs (Burlingame, CA, USA). Human umbilical vein endothelial cells and human lung microvascular endothelial cells (LMVECs) were purchased from Lonza (Allendale, NJ, USA) and EndoGRO-Media from Millipore Inc. (Billerica, MA, USA). All shRNA retroviral constructs were purchased from Origene (Rockville, MD, USA). 5-Bromo-2-deoxyuridine (BrdU) labelling and detection kit III (1144461100) was purchased from Roche (Nutley, NJ, USA).

## 2.2 Animal studies and generation of *Lpp3*$^{\Delta fl/\Delta fl}$ (aka *Lpp3*$^{ECKO}$ or *MT*) mice

Methodologies for animal care including breeding, genotyping, and collection of embryos were approved by the University of Illinois at Chicago Animal Care Committee. The animal experiments were performed conform the NIH guidelines (guide for the care and use of laboratory animals) or the guidelines from Directive 2010/63/EU of the European Parliament on the protection of animals used for scientific purposes. To investigate the role of Lpp3 in the development of the vasculature, we employed the *Cre/loxP* system and *Tie2*$^{Cre}$ transgenic animals.[28] *Tie2* is an EC-specific receptor and the promoter has mostly EC-specific expression, however, also expressed by monocytes and macrophages. Male *B6.Cg-Tg(Tek-cre)12Flv/J* and male *B6.129S4-Gt(ROSA)26Sortm1(FLP1)Dym/JRainJ*[29] mice were purchased from Jackson Labs (Bar Harbor, MN, USA), backcrossed with C57BL mice for six generations. Using mouse *Lpp3* exon-3 probe, we screened and obtained five bacterial artificial chromosomes (BAC) (RPC122-278N3, -258K13, -268N13, -268H13, -258G15; Children's Hospital Oakland Research Institute, Oakland, CA, USA). Exons 3 and 4 encode a lipid phosphatase domain and the integrin binding (RGE) sequence. Polymerase chain reaction (PCR) using BAC as template was used to generate a 3.9 kb 5′ arm of homology, a 1.2 kb 'floxed' sequence containing exons 3 and 4, and a 3.0 kb 3′ arm of homology (*Figure 1A*). These fragments were used in the construction of a gene-targeting vector. The *Lpp3* gene targeting strategy entailed incorporation of the recognition sequences for two site-specific recombinases, *Cre* and *Flp*, into the *Lpp3* gene using homologous recombination. This vector incorporates 1.8 kb fragment containing a PGK-*Neomycin* resistance cassette that is flanked by *Flippase* recognition target sites (FRT) into the intron between exons 4 and 5. Exons 3 and 4 of *Lpp3* are placed between tandem *loxP* sites, such that these coding segments can be deleted *in vivo* in a *Cre*-recombinase dependent manner (*Figure 1A*). The 5′ and 3′arms of homology are needed to allow for homologous recombination. Correctness of targeting construct was determined by DNA sequencing and restriction digests. ES cell clones were identified by PCR using *Neomycin* (*Neo*) cassette-specific primer, For-5′-*CTTCCTCGTGCTTTACGGTATC*-3′and Rev-5′-*GTAGCTAGCACAATGACAAG*-3′ (from 3′arm). Targeted ES cell clones were also confirmed by Southern blot analysis with 5′ and 3′probes (*Figure 1A*), and the targeting frequency was 8 out of 384 clones (2.0%). Aggregation, breeding of chimeras, and the germline *Lpp3*$^{loxP-Neo/+}$ were generated by inGenious Targeting Laboratories (Stony Brook, NY, USA). Male *Lpp3*$^{loxP-Neo/+}$ mice were crossed with *Rosa.Flp1*-recombinase (female) transgenic mice, which removed the neomycin cassette (*FRT-Neo-FRT*), leaving two *loxP* sites flanking exons 3 and 4, resulting in *fl-Lpp3*$^{\Delta Neo/WT}$ mice. To avoid possible confusing effects of other genetic variables in our phenotypic analyses, these mice were backcrossed for 12 generations in an isogenic strain to generate *fl-Lpp3*$^{\Delta Neo/WT}$ in C57BL background. Next, *fl-Lpp3*$^{\Delta Neo/WT}$ mice were crossed with their siblings of same genotype to produce *fl-Lpp3*$^{\Delta Neo}$/*fl-Lpp3*$^{\Delta Neo}$ (hereafter called *Lpp3*$^{fl/fl}$; 25%) of C57BL background. Finally, *Lpp3*$^{fl/fl}$ (female) were crossed with *B6.tg.Tie2*$^{Cre}$ (male) transgenic line[28] in C57BL background to generate *Lpp3*$^{\Delta fl/\Delta fl}$ (25%), henceforth called

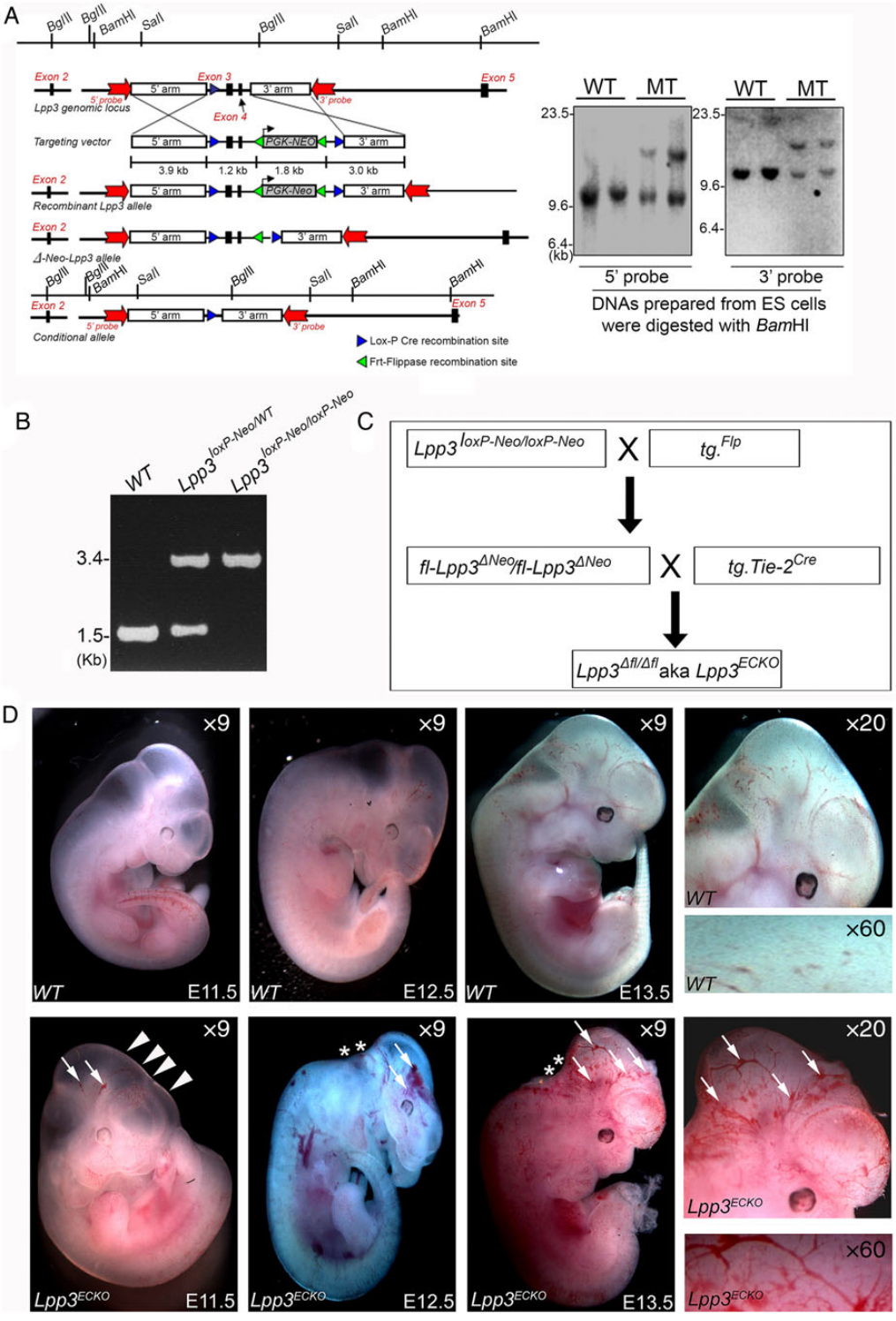


**Figure 1** Severe localized haemorrhages and lethality in *Lpp3*$^{ECKO}$ embryos. (*A*) Top left: strategy for deletion of *Lpp3* alleles and targeting vector. The *Tie2*$^{Cre}$-mediated excision of the floxed allele is expected to generate a null *Lpp3* allele in ECs. Top right panels: Southern blot analyses of DNAs from ES cells to determine homologous recombination. DNAs digested with *Bam*HI enzyme and hybridized with indicated probes. In addition to ~10.8 kb wild-type (*WT*) fragments, we show ~12.6 kb novel fragments hybridized with both 5′ and 3′ genomic repeat-free probes. (*B*) Representative images of EtBr-stained PCR-genotyping of indicated alleles. (*C*) Simplified breeding scheme used for producing *Lpp3*$^{ECKO}$ (*MT*) embryos. (*D*) Top panels: representative images of *WT* (*tg.Tie2*$^{Cre}$) embryos collected on indicated days showing normal growth and vascular development; right panel: head region of the same *WT* embryo. Bottom panels: representative images of indicated *Lpp3*$^{ECKO}$ embryo showing severe haemorrhage (white arrows). WT, wild-type; MT, mutant; Molecular weight is shown in kilobase pairs (kb). The targeting vector diagrams are not shown to exact scale. Magnifications are as shown. Images are representative of three independent experiments in which 9 (WT) and 12 (MT) separate embryos for each time points were evaluated ($n = 9–12$); for more details, please see statistics in the Methods section.

*Lpp3*$^{ECKO}$ or mutant (*MT*) embryos. All newborn mice and embryos were genotyped by PCR analyses of genomic DNAs for the presence of both wild-type (*WT*) and *MT* alleles. *B6.Tie2*$^{Cre}$ littermates were used as *WT* control. For genotyping *fl-Lpp3*$^{Neo}$/*fl-Lpp3*$^{Neo}$ and *Lpp3*$^{fl/fl}$ siblings, *Lpp3*-For-5′-*GTACTGGATCGATAGCACACACTC*-3′ and *Lpp3*-Rev-5′-*AGATACAAATAGATCTTCAAGGAC*-3′primers were used. For genotyping the *tg.Tie2*$^{Cre}$ transgene, *Cre*-For-5′-*GATATCTCACGTACTGACGG*-3′ and *Cre*-Rev-5′-*TGACCAGAGTCATCCTTAGC*-3′ primers, which amplify a 300 bp PCR product, were used.

## 2.3 Isolation of mouse ECs, BrdU incorporation assay, and microscopy

Fluorescence-activated cell sorting (FACS) and isolation of ECs from mouse embryonic stem cells and induced pluripotent stem cells have been previously described by us.[30–32] Briefly, for isolation of mouse ECs, we used anti-mouse-Flk1 (CD309) and anti-mouse-CD31 microbeads (Miltenyi Biotec GmbH, San Diego, CA, USA). Mouse embryos at developmental stage at E11.5 were collected, washed three times with cold 1 × PBS, pH 7.4; heart, lungs, brains, and livers were enzymatically dissociated in DMEM containing collagenase/dispase/0.1% trypsin/1.0 mM EDTA, for 30 min at 37°C in a $CO_2$ incubator. Cells were centrifuged for 5 min at 400 *g* at 4°C. Cell pellets were re-suspended in DMEM + DNase I (10 units/mL), passed through Falcon cell strainer with a pore size of 70 μm, and collected using 50 mL Falcon centrifuge tube. Thereafter, cells were re-suspended in DMEM and sorted with anti-Flk1-magnetic beads (Miltenyl Biotec). Flk1$^+$ cells were cultured in serum-free EndoGro medium supplemented with bFGF (10 ng/mL), VEGF (50 ng/mL), and Wnt3a (50 ng/mL) for 18 h. Next day, these cells were detached with 0.1% trypsin/EDTA and sorted again with anti-CD31-magnetic beads. Flk1$^+$/CD31$^+$ (double-positive) cells were plated at a density of 2 × 10$^4$ cells onto 0.2% gelatine coated 6-well dish in serum-free EndoGro medium supplemented with bFGF, VEGF, and Wnt3a. We also generated Lpp3-deficient ECs from *Lpp3*$^{fl/fl}$ embryos; accordingly, *Lpp3*$^{fl/fl}$ ECs were infected for 18 h with recombinant adenovirus particle encoding the *Cre/RFP*, in which the RFP signal was used to assess infection efficiency. These cells were immediately used for flow cytometry, biochemical experiments, and gene expression analyses as previously described.[30–32]

For biochemical experiments, ECs isolated from Flk1$^+$/CD31$^+$ (double-positive) cells were grown for 6 days in EndoGro media supplemented with 5% FBS; bFGF (10 ng/mL), VEGF (50 ng/mL), and Wnt3a (50 ng/mL); and insulin, transferrin, and selenium (1 × ITS, Gibco-BRL). For proliferation assays, ECs were seeded on cover slips pre-coated with 0.2% gelatine and incubated in media containing BrdU (10 μM) for overnight at 37°C in a $CO_2$ incubator, thereafter stained with anti-BrdU labelling kit (Roche). *Figure* 7A represents the timeline of BrdU experiment. For quantification, at least 10 microscopic fields were selected randomly, counted and photographed on each coverslip using Zeiss microscope and Canon power shot A640 camera supported by Canon Zoom-in software. Experiments were repeated at least three to five times, with at least three technical replicates.

## 2.4 Whole mount immunohistochemistry

After timed mating, gravid mice were euthanized by cervical dislocation.[33,34] Embryos harvested by caesarean section from E11.5, E12.5, and E13.5 were fixed in freshly prepared 2% *p*-formaldehyde in PBS for 4 h at 4°C.[32,33] Whole mount immunohistochemistry protocol has been described by Courtney Griffin lab.[35] Fixed embryos were treated with PBS containing 0.15% $H_2O_2$, 0.1% $NaN_3$ for 1 h at 4°C, thereafter incubated in blocking solution (PBS-MBT, 2% carnation dry milk, 0.2% BSA, 0.6% goat serum, and 0.1% Triton X-100 in PBS, pH 7.4) at 4°C for 1 h. Next, the samples were incubated in biotinylated rat anti-mouse CD31 antibody (1:50 in PBS-MBT) for 48 h, followed by wash in PBS-MT (PBS, pH 7.4 containing 2% carnation dry milk and 0.1% Triton X-100) for five times, 1 h each at room temperature. Next, the samples were incubated in 1:200 diluted peroxidase-labelled goat anti-rat IgG (KPL) at 4°C for overnight. Next day, samples were washed for five times in PBS-MT for 1 h each at room temperature. Peroxidase-stained embryos were visualized by using a DAB kit (Vector Labs). Stained embryos were immersed in 50% glycerol, and vascular developments of the embryos photographed using Zeiss stereo microscope at room temperature.

## 2.5 TUNEL apoptosis assay

Terminal deoxynucleotidyl transferase-mediated dUTP-biotin nick end-labelling (TUNEL) assays were performed on paraffin-embedded sections prepared from E13.5 using EC-specific VasoTACS *in situ* apoptosis detection kit (Trevigen).[36,37] For imaging and quantification, 20 microscopic fields were selected randomly, photographed with Zeiss Apotome microscope acquired using AxioVision software at room temperature. TUNEL-positive ECs were quantified in both MT and their WT littermates. Experiments were repeated at least three times.

## 2.6 Immunohistochemistry and microscopy

Staining and microscopy methods have been previously described.[19,22,30] In brief, paraffin-embedded sections prepared from E13.5 were rehydrated in graded ethanol then treated with 3% hydrogen peroxide ($H_2O_2$) for 20 min, next the samples were blocked with 5% normal goat serum diluted in 1 × PBS, pH 7.4, for 1 h. Sections were incubated in primary antibodies for 1 h (1:200 dilution, ∼2.0 μg/mL). After PBS wash, slides were incubated with appropriate secondary antibodies (dilution 1:300) for 1 h at room temperature. Stained sections were examined, images photographed with a Zeiss Apotome fluoroscope, and scored for staining intensity as previously described.[19,22,30]

## 2.7 Transmission electron microscopy

E13.5, both *WT* (*B6.tg.Tie2*$^{Cre}$ siblings) and *MT*, were fixed in 0.1 M cacodylate buffer, pH 7.4. All transmission electron microscopy (TEM) processing were carried out by the University of Illinois at Chicago Research Resources Center Electron Microscopy Service core facility. Images were recorded using JEM-1220 TEM and Erlangshen ESW1000W 785 digital camera supported by Gatan digital micrograph version 1.7.1 software.

## 2.8 Cell culture, shRNA transfection, and western blot analysis

For immunostaining, ECs were plated on coverslips and stained as previously described.[19–22] Lentivirus shRNA-mediated knockdown was performed as previously described,[29–31] and efficiency evaluated by western blot (WB) analysis. For WB, cells were solubilized in cell lysis buffer containing 20 mM Tris (pH 7.5), 1.0% Triton X-100, 0.2% NP-40, 1 mM EDTA, and 150 mM NaCl, in presence of freshly added protease inhibitors cocktail as previously described.[19,22] For quantification, signal band intensity was measured using ImageJ (NIH software). All WB images shown are representative, and the images within comparison groups are obtained from the same nitrocellulose membrane exposed to X-ray films exactly for same time.

## 2.9 Transendothelial electrical resistance assays

To assess EC monolayer barrier integrity, real-time transendothelial electrical resistance (TER) changes in EC monolayer was recorded using the ECIS system (Applied Biophysics, Troy, NY, USA) as previously described.[38,39] ECs isolated from *WT* and *MT* mice and LMVECs were plated on gold electrode (Applied Biophysics) slides for 72 h to make a uniform monolayer. ECs were then treated with *control* shRNA or *Lpp3*-shRNA. After 6 h, Lpp3-depleted cells were re-transfected with *β-catenin* cDNA or *p120-catenin* cDNA. Plates were then positioned in lock-in amplifier with a constant current of 1.0 μA supplied by a 1 V, 4000 Hz alternating current signal between the small electrode and the larger counter

electrode. The voltage between the small and the large electrodes was monitored in all of the different wells and recorded with ECIS-Applied Biophysics software. After 25 min of recording the baseline, the EC monolayers were treated with 50 nM of thrombin, thereafter thrombin-induced changes in resistance was monitored for about next 2 h. Efficiency of shRNA-mediated knockdown and cDNA transfection in HMVEC-L cells was assessed by WB (*Figure 6C*).

### 2.10 Endothelial branching point structure assay

Twenty-four-well dishes were coated with 100 μL Matrigel at 37°C for 45 min. Embryonic ECs isolated from E13.5 (as described above) were re-suspended in 200 μL of EndoGro media, thereafter plated onto the Matrigel. After attachment of ECs to the matrix, media containing bFGF (10 ng/mL), VEGF (50 ng/mL), and Wnt3a (50 ng/mL) were added. Thereafter, dishes were returned to 37°C humidified $CO_2$ incubator. After 48 h, branching point structures were evaluated, 10 random microscopic fields at ×20 magnifications were counted, and representative images were photographed with a Zeiss microscope and Canon power shot A640 camera as previously described.[22,30]

### 2.11 Quantitative real-time polymerase chain reaction assay

Total RNAs were isolated from ECs with the use of TRIzol reagent (Invitrogen); quantification and assays were performed as previously described.[30,31] Primer pairs for mouse *Lpp3*, *Lpp2*, *Cyclin-D1*, *Fibronectin*, *VE-cadherin*, *Flk1*, *Klf2*, *Klf4*, and *Hprt* were purchased from IDT DNA (Skokie, IL, USA). *Hprt* was used as an internal control to correct for the concentration of cDNA in different samples. Quantitative real-time polymerase chain reaction (qRT-PCR) was performed using Power SYBR Green RNA-to-CT™ 1-step kit (Applied Biosystems) using gene-specific primer pairs (*Table 1*).

### 2.12 Statistics

Values are means ± SEM. Statistical significances were calculated by standard *t*-test or one-way analysis of variance with Bonferroni *post hoc* test for more than two conditions, and values of $P < 0.05$ were considered statistically significant.

## 3. Results

### 3.1 *Tie2$^{cre}$*-mediated *Lpp3* deletion causes embryonic lethality in two waves and severe defects in vascular development

The *Lpp3* genomic locus, restriction sites, targeting vector schematic, and diagnostic Southern blots of targeted ES cell clones are shown in *Figure 1A*. Representative PCR genotyping results for *WT*, *Lpp3$^{loxP-Neo/WT}$*, and *Lpp3$^{loxP-Neo/loxP-Neo}$* mouse tail DNAs are shown in *Figure 1B*, and a simplified breeding scheme is shown in *Figure 1C*. To investigate the role of Lpp3 in *Tie2$^{Cre}$*-expressing cellular compartments, female *Lpp3$^{fl/fl}$* mice were crossed with male B6.*tg.Tie2$^{Cre}$* transgenic mice. *Tie2$^{Cre}$*-mediated elimination of exons 3 and 4 generated *Lpp3*-null MT embryos, which are expected to be mostly EC specific; however, Lpp3 was also expressed in non-vascular tissues. Through this breeding scheme (*Figure 1C*), we observed early on that pregnant mothers produced only 3 or 4 pups per litter, and the genotype confirmed these pups were either *Tie2$^{Cre}$* or *Lpp3$^{fl/wt}$*. Therefore, timed matings were carried out and embryos were harvested from the pregnant mothers; subsequently, these embryos were subjected to microscopic phenotypic analyses. The microscopic examination provided indication that some of the embryos were blue and some were small (Supplementary material online, *Figure S1A–D*), and these abnormal embryos died between E8.5 and E10.5 and we considered this as the first wave of lethality. Microscopic analysis of haematoxylin and eosin (H&E)-stained paraffin sections prepared from dead embryos indicated the presence of ECs and red blood cells but poorly developed cardiovascular structures. The analyses of E11.5 to E13.5 indicated that *Lpp3$^{ECKO}$* (also indicated as *MT*) embryos likely died *in utero* due to the defects in vascular structures and haemorrhage (*Figure 1D* and Supplementary material online, *Figure S1E–I*), and we attributed this event to the second wave of lethality. To confirm the loss of Lpp3 in ECs, we isolated ECs from these embryos; these ECs showed the absence of the *Lpp3* transcript or loss of the Lpp3 protein. Thus, *MT* embryos died in two waves. Genotyping of ECs isolated from these embryos confirmed

**Table 1 Oligonucleotides used for amplifying mouse transcripts through qRT-PCR**

| | Gene name | Sequence | Genbank accession number |
|---|---|---|---|
| 1 | *Lpp3* | For: 5′-TCT GAC TAC AAG CAT CAT CCT AGC-3′<br>Rev: 5′-GCT CGT CTT AGT CTT GAA GAG GTC-3′ | NM_080555.2 |
| 2 | *Lpp2* | For: 5′-CCT GCC TCA CGC TAT ATG TGC-3′<br>Rev: 5′-CAC CAA GAA GAA CTG AAC AGT GG-3′ | AF123611.1 |
| 3 | *Flk1* | For: 5′-GAA GAG CTG AAA ACT CTG GAA GAC-3′<br>Rev: 5′-ACA GAC TCC CTG CTT TTA CTG G-3′ | NM_010612.2 |
| 4 | *VE-cadherin* | For: 5′-CTG GTG GCC ATC TTC CTC T-3′<br>Rev: 5′-GCA GGA TGA TCA GCA AGG TA-3 | BC054790.1 |
| 5 | *Fibronectin* | For: 5′-CCA CAC CTA CAA CCA GTA TAC ACA-3′<br>Rev: 5′-AGC ACT CAA TGG GGC AAT TTA C-3′ | BC138421.1 |
| 6 | *Cyclin-D1* | For: 5′-CTC TTG CAT GGA AGT GTC TCC TAC-3′<br>Rev: 5′-AGG TAG GCT GAC ATG AGG AAA TC-3′ | BC044841.1 |
| 7 | *Klf2* | For: 5′-AAC TGC GGC AAG ACC TAC AC-3′<br>Rev: 5′-TCC TTC CCA GTT GCA ATG AT-3′ | NM_008452.2 |
| 8 | *Klf4* | For: 5′-ACC CAC ACT TGT GAC TAT GCA G-3′<br>Rev: 5′-AGT CAC AGT GGT AAG GTT TCT CG-3′ | NM_010637.3 |
| 9 | *Hprt* | For: 5′-GTG AAA AGG ACC TCT CGA AGT GTT-3′<br>Rev: 5′-ATA GTC AAG GGC ATA TCC AAC AAC-3′ | J00423.1 |

that heterozygote embryos appeared normal, while homozygote (*Lpp3*$^{ECKO}$) embryos did not survive beyond E13.5, as dead embryos were frequently found *in utero*, indicating late embryonic lethality. Heterozygous mice (*fl-Lpp3*$^{\Delta Neo/WT}$) appeared to be phenotypically normal, and their viability was similar to that of *WT* littermates. To perform phenotypic analyses, *WT*- and *MT*-embryos were collected at specific developmental stages (*Table 2*) and subjected to microscopic analyses. Normal vascular patterning was also seen in normal head and tails at E12.5 (Supplementary material online, *Figure S2A–C*). However, in *MT* embryos, severe haemorrhage was visible in the head region (*Figure 1D*, bottom right panels; Supplementary material online, *Figure S2D*). In addition, we observed defective sprouting of blood vessels in the tails of the *MT*-embryos but not in *WT*-tails (Supplementary material online, *Figure S2E* and *F*). These results indicated that *Tie2*$^{Cre}$-mediated *Lpp3* deletion produces embryonic lethality in two waves.

## 3.2 Embryonic lethality in *Lpp3*$^{ECKO}$ is accompanied by defects in developing blood vessels

To determine the role of Lpp3 in ECs, microscopic and histological analyses were performed. Anatomical and histological examinations of *WT* (*tg.Tie2*$^{Cre}$) and *MT* (*Lpp3*$^{ECKO}$) embryos revealed no gross abnormalities prior to E11.5. Detailed microscopic analysis of H&E-stained sections of E13.5 *MT*-embryos revealed severe haemorrhage in the brain cavity. These haemorrhages were most likely one of the main causes of embryonic death. Although it was difficult to precisely determine the primary sites of haemorrhage based on the microscopic examination, the haemorrhages appeared to extend mainly to the frontal regions of the brain cavity. To determine whether vascular leakage was due to an altered EC phenotype, we performed whole-mount staining with a monoclonal anti-CD31 antibody to visualize the vascular system (*Figure 2A–H*). Anti-CD31 staining of *MT* embryos revealed developing neovessels with patches showing haemorrhagic events inside the head region (*Figure 2B–D*). We also observed several blunt-ended vessels; however, there was no such defect in the *WT* embryos (*Figure 2A–D*). Staining with anti-CD31 showed normal vascular development in the *WT*-eye (*Figure 2E*), whereas the formation of the vascular network in the *MT*-eye (*Figure 2F*) was not as extensive as that in the *WT*-eye. The gross vascular network in the *MT*-eye seemed to be incomplete and often failed to form stable vascular network connections (*Figure 2F*). Retinal neovessel formation occurs immediately after birth, and prior to that, the hyaloid vasculature supplies the inner eye and lens; immediately after birth, these hyaloid vessels start to regress as the neovessels form. The neovessels in the *MT*-hyaloid were reduced. Anti-CD31 staining of the *MT* embryos showed haemorrhages in the early vascular plexuses (*Figure 2D*). We also found impaired vascular remodelling in the yolk sac in *Lpp3*-deficient embryos (*Figure 2G* and *H*). Trabeculation and the growth of compact wall of the myocardium are morphogenetic events that are known to be critical for the development and function of the ventricular walls. In addition, the interactions between ECs in the developing heart and adjacent cardiomyocytes provide intimate signalling cross-talk to control cardiac development, contractile activities, and rhythmicity. Since EC–cardiomyocyte interactions play a key role in cardiac growth, we stained *WT*- and *MT*-heart sections with H&E. Examination of the *WT*-heart showed the presence of apparently normal epicardium, myocardium, and endocardium, with an expected level of trabeculation and the growth of compact wall, and the presence of epicardium (*Figure 3A, B*, and *G*); in contrast, the *MT*-heart showed significantly decreased trabeculation, insufficient growth of the compact wall, and hypocellular myocardial wall defect accompanied by thin epicardium (*Figure 3C, D*, and *H*). Additional images (*Figure 3E* and *F*) represent *MT*-embryo showing decreased trabeculation and insufficient growth of compact wall. Together, these results indicate that the *Tie2*$^{Cre}$-mediated deletion of *Lpp3* affects embryonic cardiovascular development.

**Table 2 After timed matings, embryos were collected, and their viability and genotypes determined**

| | Days old | WT | HT (hetero) | MT | Total |
|---|---|---|---|---|---|
| 1 | E9.5 | 34 | 98 | 26 | 158 |
| 2 | E10.5 | 15 | 31 | 18[a] | 64 |
| 3 | E11.5 | 30 | 56 | 12[a] | 98 |
| 4 | E12.5 | 12 | 26 | 8[a] | 46 |
| 5 | E13.5 | 8 | 15 | 6[a] | 29 |

[a]Embryos that appeared macroscopically abnormal such as small in size and haemorrhagic, and sometimes resorbed.

## 3.3 *Lpp3*-deficient ECs show increased susceptibility to apoptosis

To determine if the vascular defects observed in *MT* (*Lpp3*$^{ECKO}$) embryos were due to EC apoptosis, paraffin-embedded sections of E13.5 *WT* (*tg.Tie2*$^{Cre}$ embryo) and *MT* embryos were subjected to immunochemical staining (*Figure 4A–H*). *WT*-embryos showed normal (basal) apoptosis (*Figure 4A, C, E*, and *I*), whereas *MT* embryos exhibited a 40 $\pm$ 4.5% increase in TUNEL$^{+}$ ECs (*Figure 4B, D, F*, and *I*) in the head region, where vascular leakage and haemorrhagic events were detected. At higher magnification, the WT-sections showed very few TUNEL$^{+}$ ECs, whereas in MT-sections, TUNEL$^{-}$ positive cells were mostly ECs (*Figure 4H*). Although VasoTac primarily detects apoptotic ECs, it may also stain smooth muscle cells; nevertheless, *Tie2*$^{Cre}$-mediated *Lpp3* deletion likely also altered smooth muscle cell survival. Next, we isolated ECs from *Tie2*$^{Cre}$ (*WT*) or *Lpp3*$^{fl/fl}$ embryos cultured for 4 days. Adenovirus particles encoding Cre/eRFP (red fluorescent protein) were added to these cells and cell extracts prepared after 18 h of infection. The basal expression of the proapoptotic mediator p53 and its target p21 protein was low in *WT*-ECs, whereas in *MT*-ECs, their expression levels increased (*Figure 4J*). We also analysed *WT* and *MT* protein lysates for the presence of Flk1 and Cre; the findings provided information regarding EC characteristics and Cre expression levels (*Figure 4J*). To examine EC integrity, we performed TEM analysis (*Figure 4K*). TEM analyses of *WT*-sections revealed normal ECs with intact vascular walls (*Figure 4K*), whereas MT-sections displayed occurrence of membrane blebbing, condensed nuclei, and (*Figure 4K*, white arrowheads) and near-apoptotic ECs (*Figure 4*, blue asterisk). In addition, staining of lung tissue sections prepared from E13.5 *WT*- (Supplementary material online, *Figure S3A*, top panels) and *MT*-sections (Supplementary material online, *Figure S3B*, bottom panels) with anti-cleaved caspase-3 showed the presence of apoptotic vascular cells in *MT*-embryos (Supplementary material online, *Figure S3B* and *C*). Furthermore, purified *MT*-ECs showed strongly positive staining for anti-cleaved caspase-3 (data not shown).

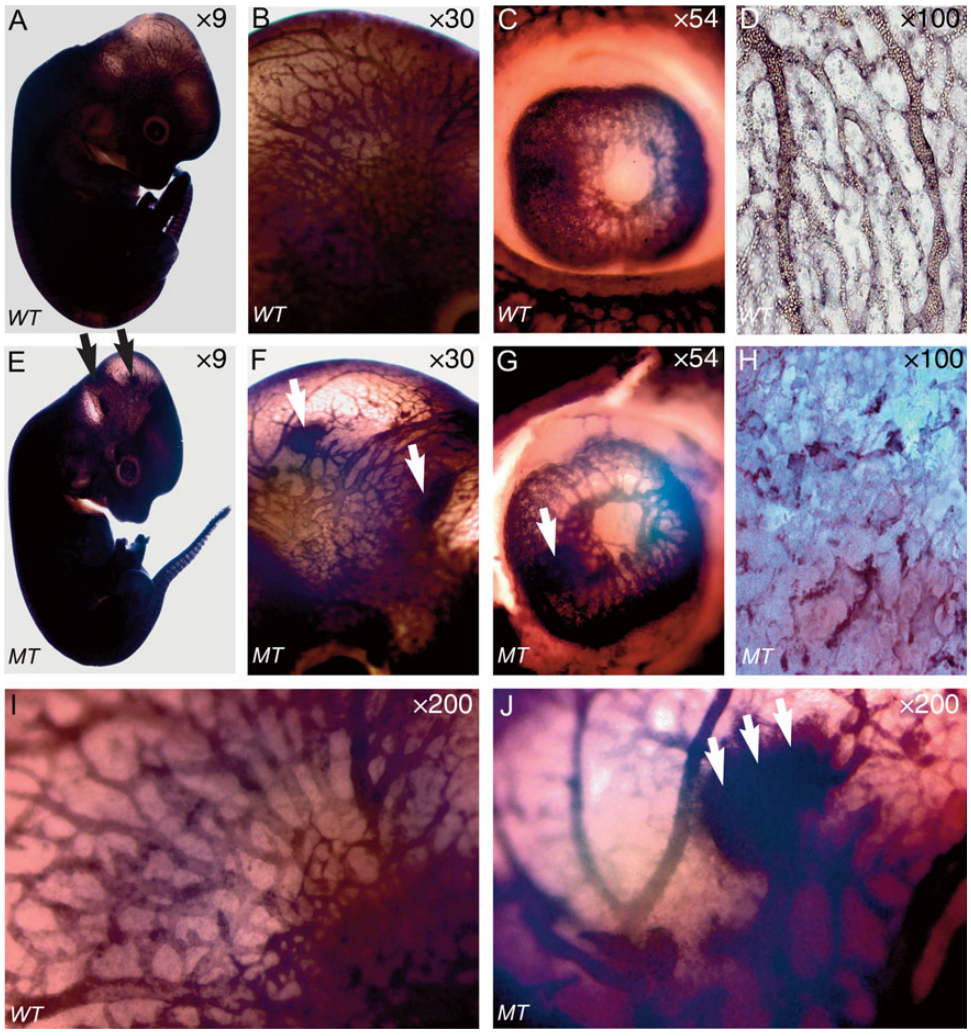


**Figure 2** CD31 staining reveals leaky vasculature in developing *Lpp3*$^{ECKO}$ (*MT*) embryos. (*A*) *WT* mice embryo reveals normal developing neovessels; (*B*) magnified image of the head region of *WT* embryo; (*C*) magnified images of eye hyaloid vasculature in *WT* embryo; (*D*) normal vascular patterning of the yolk sac of *WT* embryo with normal branching point networks. (*E*) *MT* embryo reveals abnormal neovessels with haemorrhage (black arrows); (*F*) *MT* embryos with vascular leakage (arrows). *MT* embryos show defects in developing vasculature (white arrows). (*H*) MT yolk sac shows lack of vascular network formation. (*I* and *J*) Magnified images of vascular structures. Experiments were carried out at least two times. Magnifications are as shown. Images are representative of three independent experiments in which 6 (WT) and 9 (MT) separate embryos were stained with anti-CD31 ($n = 6–9$).

## 3.4 Decreased VE-cadherin and fibronectin expression in *Lpp3*$^{ECKO}$ ECs

To determine the role of LPP3 in cardiovascular patterning defects, we prepared sections of large blood vessels from E13.5 mouse embryos and immunostained them with anti-VE-cadherin and anti-fibronectin antibodies. As opposed to *WT*-sections, *MT*-sections showed decreased expression of VE-cadherin and reduced deposition of fibronectin; however, no appreciable alteration was observed with anti-CD31 (*Figure 5A–D*).

Next, we isolated ECs from E12.5 *WT*- and *MT*-embryos as described in the methods; the procedure was as reported in previous studies.[30–32] Endothelial identity was confirmed using flow cytometry analysis with control IgG, anti-CD31, and anti-Flk1 antibodies (*Figure 5E*). Next, using these isolated ECs, we performed a qRT-PCR assay to identify the target genes involved in Lpp3-regulated angiogenesis. After overnight growth factor starvation, total mRNAs were prepared from *WT*- and *MT*-ECs, and the expression levels of candidate genes and EC genes in these cells were determined. Notably, in this assay (*Figure 5F*), the basal expression of *Lpp3*, *Lpp2*, *Cyclin-D1*, *Flk1*, *VE-cadherin*, and *fibronectin* was readily detectable in *WT*-ECs, whereas *MT*-ECs exhibited reduced expression of *Lpp3*, *Cyclin-D1*, *VE-cadherin*, and *fibronectin* in the ECs that were cultured under serum-free and growth factor-free culture conditions (*Figure 5F*). This result suggests that *Cyclin-D1*, *VE-cadherin*, and *fibronectin* are regulated directly or indirectly by Lpp3. The morphology of *WT*- and *MT*-ECs is shown in *Figure 5G*.

## 3.5 Loss of EC-*Lpp3* results in increased susceptibility to endothelial barrier disruption

The interaction of cytoplasmic domain of VE-cadherin with β-catenin and p120ctn proteins are critical for neovessel stability and

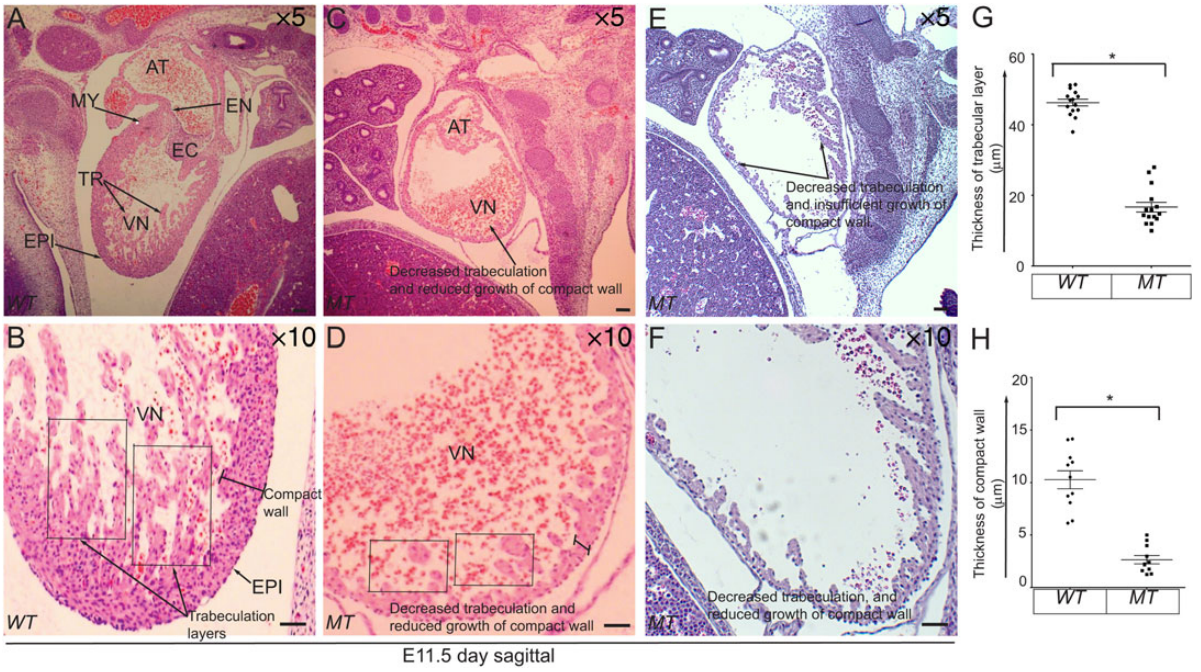


**Figure 3** Insufficient trabeculation and decreased growth of the compact wall in *Lpp3*$^{ECKO}$ heart. H&E staining of sagittal sections heart prepared from E11.5-day-old embryos showed insufficient development of heart associated with decreased trabeculation and reduced growth of the compact wall in *MT*-embryos. (*A* and *B*) Normal heart development associated with normal growth of the atrium (AT) and the ventricle (VN) that are separated by the endocardial cushion (EC), and presence of trabeculation and normal growth of the compact wall in *WT*-embryo heart. The outer myocardial (MY) muscle and inner endocardial (EN) endothelium are discernible, and epicardium (EPI) is well developed. Decorative myocardial trabeculae (TR) are lined by a layer of endocardial ECs. (*C* and *D*) *MT*-embryo section through the heart shows reduced trabeculation and decreased growth of the compact wall resulting in insufficient cardiac development. *(E* and *F*) Another example of defective cardiac development associated with decreased trabeculation and decreased growth of the compact wall in *MT*-embryo. (*G*) Quantification of trabeculation layer (μm). (*H*) Quantification of thickness of compact wall (μm). For quantifications, 9–12 embryos were used for WT- ($n = 9$) and MT-heart ($n = 12$) sections. From each embryo, at least three H&E stained slides were prepared and examined through ×10 objectives. Each data point in the bar graph (*Figure 3G* and *H*) represents average of three slides obtained from same embryo (for additional details, please see statistics in the Methods section). *$P < 0.05$ vs. control.

endothelial barrier function.[3,4,6] While examining H&E sections of *MT* embryos, we also observed defective lung development (data not shown), which was likely due to defective EC integrity. To test the hypothesis that the loss of LPP3 results in increased vascular permeability of LMVECs, we plated LMVECs on gold-plated electrodes and allowed them to form a confluent monolayer; subsequently, a knockdown experiment was performed using the *control shRNA* and the *LPP3-shRNA* retroviral particles. The timeline of the experiment is shown in *Figure 6A*. As shown in *Figure 6B*, in one group of LPP3-depleted LMVECs, *β-catenin cDNA* was transfected transiently, whereas in the second group, *p120ctn cDNA* was transfected. In LPP3-depleted LMVECs, the baseline TER value and the permeability decreased, whereas in the control group, no appreciable changes were observed. The addition of thrombin (50 nM) to the LMVEC monolayer decreased the resistance, which gradually returned to baseline, indicating re-annealing of the LMVEC monolayer. Thrombin significantly decreased the TER of LMVEC monolayers after *LPP3* knockdown (*Figure 6B*); this defect was partially restored following transfection with a retrovirus encoding *β-catenin cDNA*, whereas *p120ctn* had no effect. The efficiencies of knockdown and cDNA transfections were analysed by WB (*Figure 6C*). The data suggest that the loss of *Lpp3* is incompatible with vascular EC barrier integrity, which can be rescued, in part, by β-catenin but not by p120ctn.

## 3.6 β-catenin, but not p120ctn, restores the effect of Lpp3 loss

Proliferation of ECs and the formation of branching point structures represent hallmarks of angiogenesis. To determine if LPP3 plays a role in these processes, ECs isolated from E13.5 *MT* and *WT* embryos were subjected to cell proliferation assays; the timeline of this experiment is shown in *Figure 7A*. As opposed to 42 ± 4.5% incorporation of BrdU observed in *WT*-ECs, *MT*-ECs showed only 11 ± 3.25% BrdU incorporation (*Figure 7B* and *D*). However, the decreased proliferation was rescued, in part, by transfection of *MT*-ECs with a retrovirus particle encoding *β-catenin cDNA* (*Figure 7B* and *E*). Representative images of BrdU incorporation assays are shown in *Figure 7C–E*. WB analyses showed decrease in β-catenin, VE-cadherin, cyclin-D1, and fibronectin expression in the *MT*-ECs; however, the effect of Lpp3 loss was partially restored by *β-catenin cDNA* transfection (*Figure 7F*). The use of the anti-fibronectin antibody revealed immature (fast-moving) forms of fibronectin polypeptide species, raising the possibility that LPP3 regulates the maturation of fibronectin at the translational level as well. However, we did not investigate this phenomenon in detail. The expression of the Cre enzyme was determined using anti-Cre antibodies and equal loading with anti-GAPDH antibodies (*Figure 7F*, lowermost panels). The relative fold change in WB signal intensities is shown in *Figure 7G*. Next, we plated *WT*-ECs, *MT*-ECs, and *MT*-ECs receiving *β-catenin cDNA*

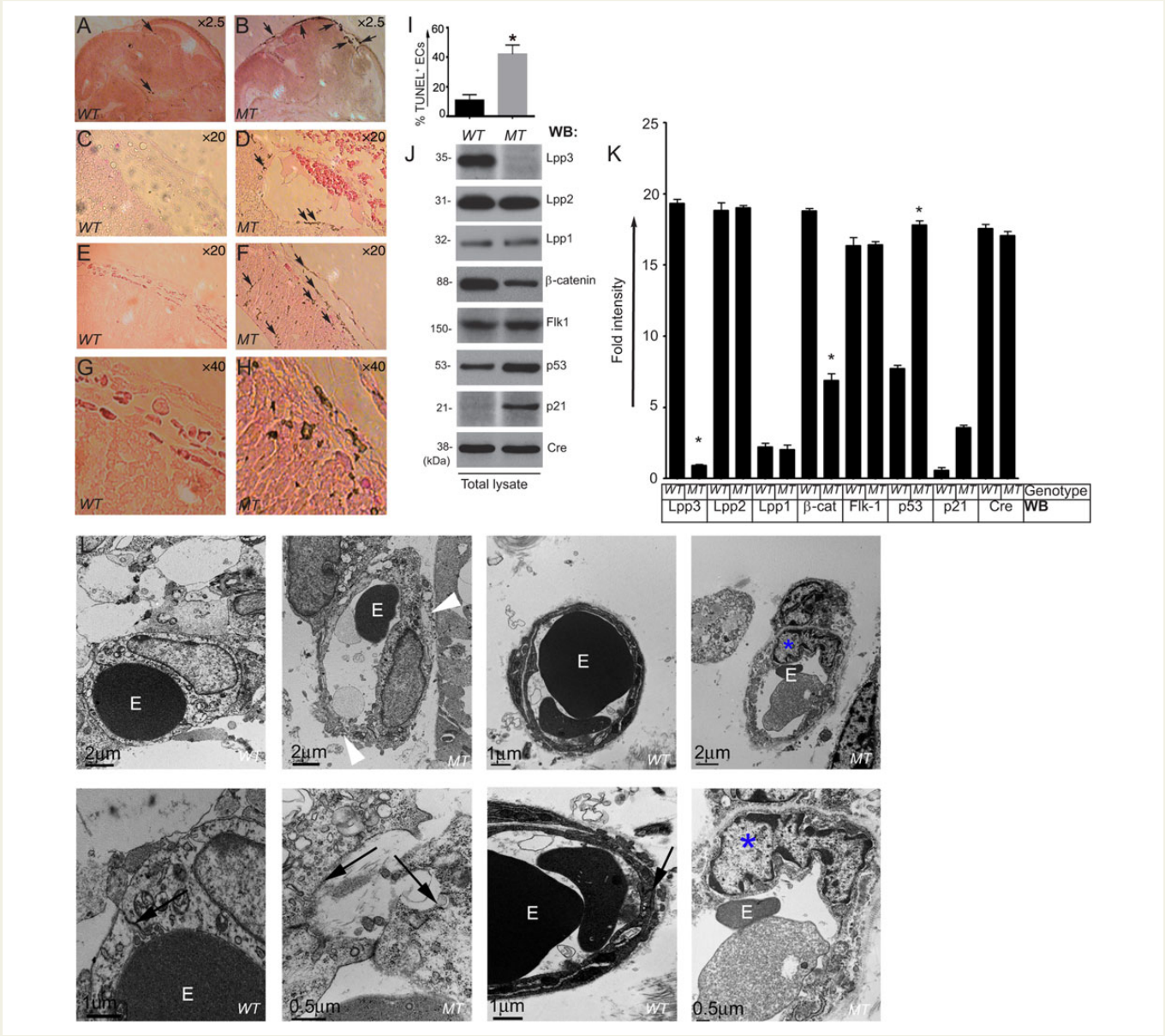


**Figure 4** Presence of apoptotic ECs in developing E13.5 *Lpp3*$^{ECKO}$ (*MT*) embryos. (*A*) Very few apoptotic ECs are seen in *WT* (*tg.Tie2*$^{Cre}$) E13.5 embryo. (*B*) *MT* sections show numerous apoptotic ECs in the haemorrhagic region of the head. (*C*) Normal developing blood vessels in head region of *WT* embryo. (*D*) *MT* embryo shows presence of apoptotic ECs (arrows). (*E*) *WT* embryo section showing normal microvessels. (*F*) Apoptotic ECs lining the microvessels (black arrows). (*G* and *H*) Magnified images of E and F, respectively. Dark brown stainings indicate apoptotic ECs. (*I*) Quantification of apoptotic ECs. The data represent the mean ± SEM. $n = 5$ from three independent experiments. (*J*) Relative abundance of proteins in WT-ECs and MT-ECs total lysates were analysed by WB with indicated antibodies. Equal loading of proteins across the lanes were determined with anti-Cre antibody. (*K*) Densitometric quantifications of WB signal intensity, fold change from the background (background was considered as one-fold) are shown, $n = 4–5$. *$P < 0.05$, by the Student unpaired *t*-test. The data are the means ± SEM. (*L*) Top panels: TEM analyses of the microvessels in (E13.5) *WT*- and *MT*-embryos. ECs lining the endothelium of *MT* embryos show membrane blabbing (white arrows), and presence of intercellular gaps in between adjacent ECs. Bottom panels: magnified view of the blood vessels showing altered EC–EC adhesion structures and frequently shows condensed and fragmented nuclei (*). Magnifications are as shown. E, erythrocyte. Images are representative of three independent experiments in which 9–12 separate embryos were evaluated ($n = 9–12$).

onto Matrigel to examine the ability of these cells to form branching point structures. The strategy and the timeline of formation of the branching point structures are shown in *Figure 7H*. As shown in *Figure 7I* and *J*, as expected *WT*-ECs formed branching point structures, whereas *MT*-ECs (*Lpp3*$^{ECKO}$) showed a significantly reduced number of branching point structures over the same period (*Figure 7I* and *K*). Transfection with retrovirus particles encoding *β-catenin cDNA*- into *MT*-ECs restored the ability of *MT*-ECs to form branching point structures, but not to the same extent as that for *WT*-ECs (*Figure 7I* and *L*).

## 4. Discussion

Here, we showed that Lpp3 is essential for some aspects of cardiovascular development in the mouse embryo between E8.5 and E13.5.

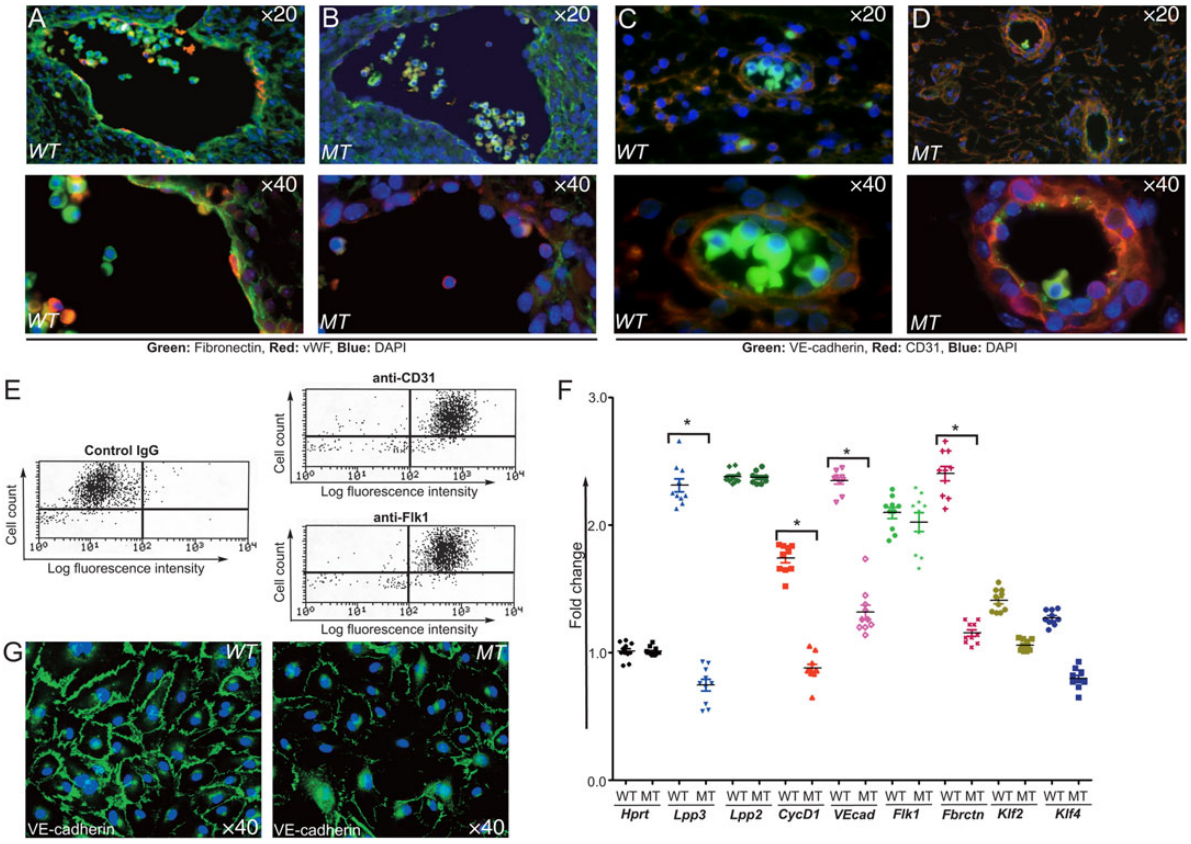


**Figure 5** Decreased VE-cadherin and fibronectin in E13.5 *Lpp3*$^{ECKO}$. Sections prepared from the head region of E13.5 were stained with (*A*) anti-fibronectin (green) decorated mostly the basement membrane of the vascular wall. (*B*) Decreased fibronectin immunoreactivity in the *MT* section. (*C*) VE-cadherin and CD31 were detectable in the *WT* section. (*D*) Decreased VE-cadherin immunoreactivity in the *MT* section. The lower panels represent magnified images (×40) of top panel pictures. ECs were isolated from E13.5-day-old embryos using anti-Flk1 and anti-CD31$^{+}$ beads (please see methods) and as previously described.[30–32]. (*E*) Purity of isolated mouse ECs: representative FACS profiles of mouse ECs with control IgG, anti-CD31, and anti-Flk1 antibodies. (*F*) qRT-PCR data obtained from *WT*- and *MT*-ECs are as shown. Primer pairs for used for amplifying *Hprt*, *Lpp3*, *Lpp2*, *CycD1* (*Cyclin-D1*), *VEcad* (*VE-cadherin*), *Flk1*, *Fbrctn* (*fibronectin*), *Klf2*, and *Klf4* genes are listed in *Table 1*. Values are expressed as the mean ± SEM. Experiments were performed three times independently with three technical triplicates and expression normalized to *Hprt*. *$P < 0.05$, $n = 9–10$ embryos, '*n*' represents the number of individual embryos used. (*G*) Representative images of CD31$^{+}$ and Flk1$^{+}$ *WT*- and *MT*-ECs cultured for 4 days on gelatine-coated glass coverslips were stained with anti-VE-cadherin antibody (green) and DAPI (nucleus, blue); compared with *WT*-ECs, *MT*-ECs expressed reduced VE-cadherin. Magnifications are as shown.

Embryos lacking EC-Lpp3 developed cardiovascular defects that were different from those described in *Lpp3*-deletion experiments,[24–27] demonstrating that signalling pathways mediated through Lpp3 are crucial for normal embryonic development. Specifically, (i) EC-*Lpp3* deficiency led to embryonic deaths in two waves; (ii) *Lpp3*$^{ECKO}$ embryos developed haemorrhages and apoptotic ECs secondary to the loss of barrier integrity; (iii) in *Lpp3*$^{ECKO}$ ECs, the expression of *cyclin-D1*, *VE-cadherin*, *fibronectin*, *Klf2*, and *Klf4* decreased; and (iv) the re-expression of *β-catenin* in *Lpp3*$^{ECKO}$ ECs partially restored the effect of the loss of LPP3, whereas *p120ctn* did not. Together, these results indicate a crucially important role for LPP3 in the maintenance of EC barrier function and angiogenesis.

The expression of Lpp3 is seen in ECs at E8.5 in several different vascular bed.[24] In cultured cells, LPP3 is predominantly localized at the cell–cell junctions to maintain the steady-state levels of S1P.[18,19] We used *Tie2*$^{Cre}$ because it is a well-established system, the endothelial expression of *Tie2* is known, and its strong expression in ECs occurs as early as E8.5,[40–42] but also expressed by a subset of monocytes and macrophages, and may also be by mesenchymal cells.[28] However, what might be the reason(s) for the embryonic deaths in two waves? One could surmise that the variable level of expression of *Tie2*$^{Cre}$ likely contributed to the embryonic lethality in two waves, that is to say, the first wave of lethality (with severe phenotype) could have been due to uniform and robust nature of *Tie2*$^{Cre}$ expression throughout all vascular bed. Conversely, the expression of *Tie2*$^{Cre}$ could have been delayed in embryos that displayed mild phenotype. Alternatively, the simplest explanation could be a spectrum of penetrance causing severe and mild phenotypes. In this regard, Escalante-Alcalde *et al.* described *Lpp3*$^{-/-}$ embryonic deaths associated with two distinct phenotypes, one '*Fused*/Axin deficiency-like' and the other 'frizzled5 deficiency-like' phenotypes, but their study did not elaborate the exact biochemical mechanisms responsible for these two phenotypes.[24] However, we addressed the ability of LPP3 to titrate β-catenin signalling activities in (i) sub-confluent ECs, LPP3 activated β-catenin signalling, but (ii) confluent ECs, LPP3 down-regulated β-catenin signalling.[22] Here, we show that LPP3 is a positive regulator of cardiovascular development and

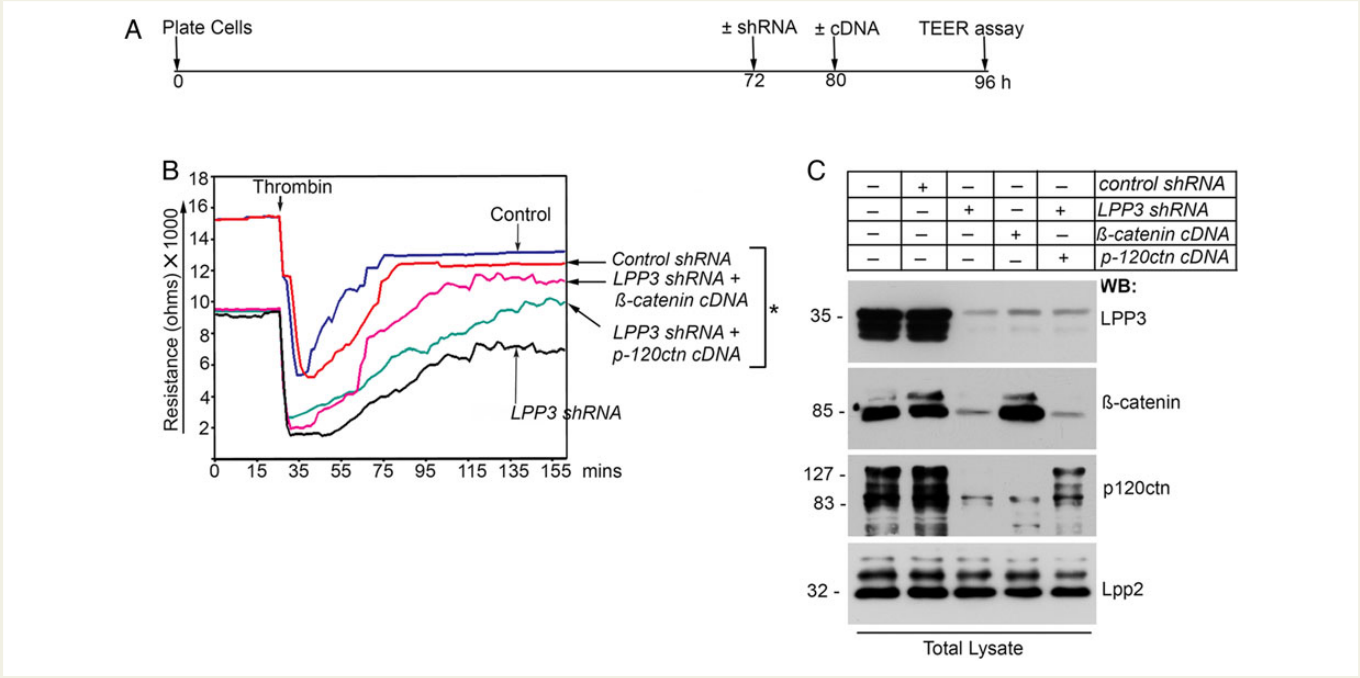


**Figure 6** *LPP3*-knockdown results in increased vascular endothelial cell permeability. (*A*) Timeline of the knockdown, β-catenin cDNA transfection, and TER assay. (*B*) LPP3-depletion results in decreased TER and increased LMVECs barrier disruption, whereas no change was observed in LMVECs receiving control *shRNA*. Following transfection of *β-catenin cDNA* into LPP3-depleted LMVECs, the TER level was restored nearly to control group, while the transfection with *p120-catenin cDNA* into LPP3-depleted LMVECs had only a modest effect. Experiments were carried out in triplicates and repeated at least three times; $*P < 0.05$. (*C*) The efficiency of *Lpp3*-knockdown was assessed by WB with the indicated antibodies. Experiments were repeated at least three times with similar results.

that it is an essential enzyme; we also provide a new mechanism of regulation of apoptosis by LPP3 and EC barrier integrity via β-catenin signalling activities. Most importantly, a subset of embryos showed a decrease in EC proliferation, accompanied by increased apoptosis, and defects in heart development that were likely secondary to defective EC behaviour. A defect in branching is also likely due to reduced EC migration and inability to form cell–cell adhesion structures. We also observed thickened blood vessels, but these effects were not statistically significant. At times, the *Lpp3*$^{ECKO}$ embryos exhibited large avascular regions between blood vessels. The lack of productive angiogenesis suggested that the reciprocal relationship between the levels of cell proliferation and apoptosis, which entails the survival mechanism, is controlled by LPP3. To our knowledge, this study is the first to demonstrate the critical role of LPP3 in the regulation of blood vessel development between E11.5 and E13.5.

Neovessel growth and remodelling during embryonic development are regulated by precise signals that determine the orderly nature of angiogenesis. *Tie2*$^{Cre}$-mediated deletion of *Lpp3* in ECs and haematopoietic cells in mice resulted in embryonic lethality. A significant number of *Lpp3*$^{ECKO}$ embryos died within E11.5–E13.5, and genotyping of ECs collected from these embryos indicated that the expression of Lpp3 was lost, with no appreciable changes in Lpp2 or Lpp1 levels. LPP2 protein levels also did not change in Lpp3-deficient ECs, suggesting that LPP2 cannot compensate for the loss of LPP3. We observed an appreciable number of abnormal embryos at E8.5–10.5 (first wave of lethality); however, detailed analysis of these embryos was difficult due to their small size and fragility. Visual examination of these embryos revealed the presence of blood vessel disruption and localized haemorrhages. CD31 staining revealed the presence of ECs in the *WT*- and *MT*-embryos. CD31 staining also confirmed the presence of haemorrhage and defective neovessels in the *Lpp3*$^{ECKO}$ embryos. H&E staining confirmed the presence of defective blood vessels. However, we could not establish the precise haemorrhage or vascular leakage sites. Therefore, we carried out immunofluorescence staining using EC markers. Staining paraffin-embedded sections and fixed cultured cells with antibodies has some limitations in that the specificity and the avidity of each antibody are different and the epitope(s) are often not fully exposed. Thus, to limit over-interpretation of our data, we used only those antibodies that have been used in many studies. With the use of CD31 staining, it was clear that ECs were present in the *Lpp3*$^{ECKO}$ embryos; however, the angiogenic activities of these cells were limited. We observed decreased fibronectin and VE-cadherin levels in the *Lpp3*$^{ECKO}$ embryo sections. Staining with anti-smooth muscle α-actin antibodies was inconclusive (data not shown).

During angiogenesis, dynamic sprouting ensures that ECs are in contact with each other, e.g. via VE-cadherin-mediated AJs, and it requires the presence of appropriate ECM proteins such as fibronectin. Sprouting ECs secrete high levels of fibronectin[1,2]; however, fibronectin is also secreted by several other cell types. Fibronectin is a multifunctional ECM protein, as it not only presents the RGD sequence to integrins but also signals through the FAK and Shc pathways.[43] As fibronectin and VE-cadherin proteins regulate multiple aspects of angiogenesis and EC barrier integrity, decreased secretion of fibronectin by Lpp3-defecient ECs could impede adhesion events and integrin signalling, which might induce EC apoptosis.[1–5,43] Thus, the observed phenotype of increased permeability and haemorrhage in MT embryos is consistent with known

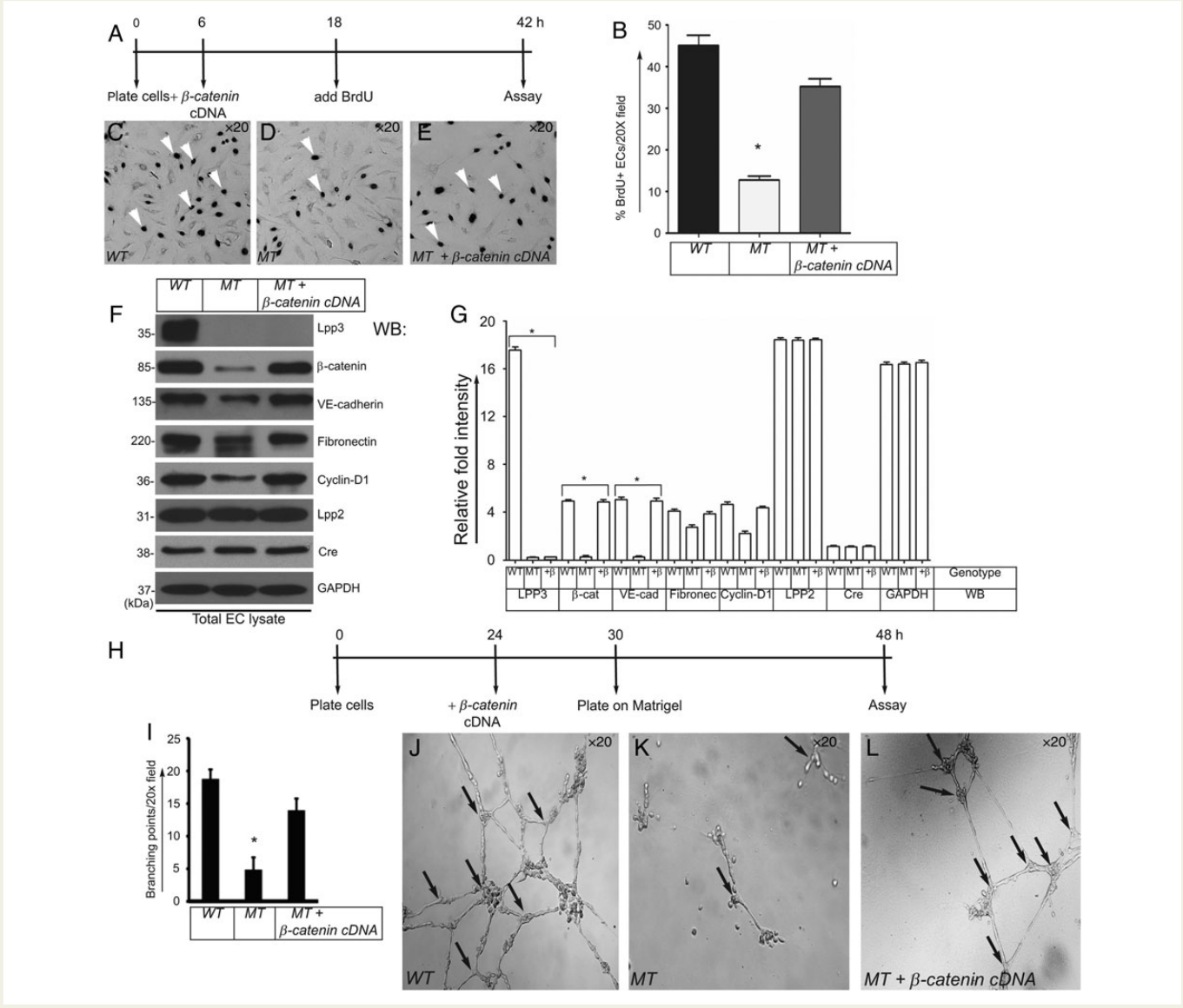


**Figure 7** Loss of Lpp3 results in decreased angiogenic activities of ECs. (*A*) The timeline of the BrdU incorporation experiment. Flk1$^+$ and CD31$^+$ ECs isolated from (E13.5) *WT*- and *MT*-embryos as described in Methods were subjected to BrdU assay. (*B*) Quantification of BrdU$^+$ ECs was performed on *WT*, *MT*, and *MT*-ECs transfected with β-catenin cDNA. White arrowheads indicate BrdU$^+$ ECs. ECs were lightly counterstained with eosin. Data represent mean ± SEM. $n = 3–5$, $^*P < 0.05$ vs. control. Experiments were repeated three times with triplicates. (*C–E*) Representative images of the BrdU assay. (*F*) WB analyses of total lysates prepared from *WT*, *MT*, *MT*-ECs receiving β-catenin cDNA ECs were subjected to immunoblotting analyses with indicated antibodies. Molecular weights, in kilo Daltons (kDa). (*G*) Densitometric quantifications of WB signal fold intensity change from Cre (Cre expression level was considered as one-fold) are shown, $n = 5–6$. $^*P < 0.05$, by the Student unpaired *t*-test. The data are the means ± SEM. (*H*) Strategy and timeline of formation of endothelial branching point structure assay. (*I*) Quantification of branching point structures. Data are expressed as a percentage of branching points ($n = 3$, $^*P < 0.05$ vs. control). The experiments were repeated three times with the use of triplicate wells. (*J–L*) Representative phase contrast images of branching point structures of CD31$^+$ and Flk1$^+$ *WT*-, *MT*- and *MT*-ECs receiving *β-catenin* cDNA ($2 \times 10^5$) were plated onto growth factor reduced Matrigel in the presence of bFGF (10 ng/mL) and VEGF$^{165}$ (50 ng/mL). After 18 h, the numbers of branching points were enumerated in 10 randomly selected ×20 microscopic fields. Magnifications are as shown. The black arrows indicate branching points. Experiments were repeated at least three times with similar results.

functions of fibronectin and VE-cadherin. The loss of EC-Lpp3 decreased the expression of β-catenin and VE-cadherin, two of the most important adhesion proteins that are critical for EC integrity and survival. Although Lpp2 and Lpp3 share the same substrates, the Lpp2 level remained unchanged, suggesting that the loss of Lpp3 in ECs cannot be compensated by Lpp2. Most studies have described LPP3 enzymatic activity, and because it has numerous substrates, the rescue experiments are problematic. However, β-catenin could rescue the effect of Lpp3 loss. These results indicate that β-catenin not only mediated Wnt signalling but also mediated cell–cell adhesion by binding to the cytoplasmic domain of VE-cadherin.

How does LPP3 stabilize β-catenin? This question has been previously addressed by us[22]; therefore, we focused on delineating the downstream events after β-catenin stabilization. Thus, the *Lpp3*

deletion primarily altered ECs behaviour due to decreased levels of β-catenin and VE-cadherin proteins and decreased expression of *Cyclin-D1*, *VE-cadherin*, *fibronectin*, *Klf2*, and *Klf4* genes. Because β-catenin is involved in cell adhesion and has the ability to act as a transcriptional regulator, it has been difficult to uncouple the control of transcriptional activities from that of cell adhesion events. Therefore, we were not surprised to find decreased expression of *Cyclin-D1*, *VE-cadherin*, *Fibronectin*, *Klf4*, and *Klf2* genes that are known downstream targets of β-catenin transcriptional activities. Thus, we postulate that Lpp3 deficiency in the vasculature decreases the expression of these genes below the optimal level that is required for normal EC development, as LPP3 likely regulates endothelial responses to athero-relevant haemodynamic forces.[44,45] Our study provides evidence that Lpp3, at least in ECs and in a subset of haematopoietic cells, plays a pro-survival role in the formation of neovessels during embryonic development. MT-embryos frequently showed striking cardiac defects. MT hearts were poorly developed as only intact structure in these hearts was the thin epicardium; importantly, in the MT-embryos, the myocardium and the endocardium were less developed, with thin ventricular wall and the cardiac cushions clearly absent. The observed insufficient myocardial trabeculation and decreased compact wall were likely to be caused by reduced β-catenin signalling and fibronectin secreted by the $Lpp3^{ECKO}$ ECs, and due to the disruption of blood vessel formation. Fibronectin deposition and assembly are required for cardiomyocyte migration and proliferation.[1,2,46,47] Fibronectin-mediated α4-integrin signalling has also been shown to control cardiac development.[48] Because endothelial cardiomyocyte interaction is also required for normal cardiac development and growth, EC death may affect cardiomyocyte survival and growth. Recently, S1P has been suggested to act as a negative regulator of angiogenesis at some point during embryonic development.[49,50] We observed that the $Lpp3^{ECKO}$ resemble $Cattnb^{fl/fl}$::$tie2^{Cre}$ embryos in their timing of lethality and head haemorrhage phenotype.[5] Thus, it would be interesting to examine if genetic overexpression of EC *β-catenin in vivo* (i.e., $Cattnb^{lox(ex3)/lox(ex3)}$) could rescue any of the haemorrhage or other vascular defects seen in $Lpp3^{ECKO}$. Future studies should address this intriguing question. Taken together, our study illuminates a crucially important function of LPP3 in ECs as a positive modifier of cardiovascular development.

Three independent genome-wide association study revealed a link between a frequently occurring variation in the *LPP3* (*PPAP2b*) loci and an increased risk of coronary artery disease.[51–53] Recent review articles have described the putative role of LPP3 to increased risk of cardiovascular disease.[44,54] Thus, the results presented in this study indicate that the loss of Lpp3 in ECs and in a subset of *Tie2*-expressing haematopoietic cells impairs the development of functional vasculature. Importantly, we demonstrate that Lpp3 is a modifier of normal embryonic blood vessel development. Our study also reveals an unusual mechanism of a lysolipid phosphatase in the regulation of vascular development; therefore, we propose that LPP3 acts as a 'gatekeeper' of normal EC homeostasis.

# Supplementary material

Supplementary material is available at *Cardiovascular Research* online.

## Acknowledgements

The authors thank the Research Histology and Tissue Imaging Core (RHTIC) for histological slide preparation and staining and the Animal Care Committee and the Veterinary staffs at the University of Illinois at Chicago, IL, USA for their help with animal experiments at the vivarium. Sakina Petiwala provided excellent technical support.

**Conflict of interest**: none declared.

## Funding

The study was supported by National Institutes of Health grants (HL079356), American Heart Association (AHA) (GRNT25710129) and by the University of Illinois, Chicago (UIC) Center for Clinical and Translational Science (CCTS) Award Number UL1RR029879 from the National Center for Research Resources to K.K.W. and AHA pre-doctoral fellowships to J.B. and E.E.L. Funding to pay the Open Access publication charges for this article was provided by K.K.W.

## References

1. Watt FM, Hodivala KJ. Cell adhesion. Fibronectin and integrin knockouts come unstuck. *Curr Biol* 1994;**4**:270–272.
2. Astrof S, Crowley D, Hynes RO. Multiple cardiovascular defects caused by the absence of alternatively spliced segments of fibronectin. *Dev Biol* 2007;**311**:11–24.
3. Gory-Fauré S, Prandini MH, Pointu H, Roullot V, Pignot-Paintrand I, Vernet M, Huber P. Role of vascular endothelial-cadherin in vascular morphogenesis. *Development* 1999;**126**:2093–2102.
4. Carmeliet P, Lampugnani MG, Moons L, Breviario F, Compernolle V, Bono F, Balconi G, Spagnuolo R, Oosthuyse B, Dewerchin M, Zanetti A, Angellilo A, Mattot V, Nuyens D, Lutgens E, Clotman F, de Ruiter MC, Gittenberger-de Groot A, Poelmann R, Lupu F, Herbert JM, Collen D, Dejana E. Targeted deficiency or cytosolic truncation of the VE-cadherin gene in mice impairs VEGF-mediated endothelial survival and angiogenesis. *Cell* 1999;**98**:147–157.
5. Cattelino A, Liebner S, Gallini R, Zanetti A, Balconi G, Corsi A, Bianco P, Wolburg H, Moore R, Oreda B, Kemler R, Dejana E. The conditional inactivation of the beta-catenin gene in endothelial cells causes a defective vascular pattern and increased vascular fragility. *J Cell Biol* 2003;**162**:1111–1122.
6. Vandenbroucke E, Mehta D, Minshall R, Malik AB. Regulation of endothelial junctional permeability. *Ann NY Acad Sci* 2008;**1123**:134–145.
7. Clevers H. Wnt/beta-catenin signaling in development and disease. *Cell* 2006;**127**:469–480.
8. Corada M, Nyqvist D, Orsenigo F, Caprini A, Giampietro C, Taketo MM, Iruela-Arispe ML, Adams RH, Dejana E. The Wnt/beta-catenin pathway modulates vascular remodeling and specification by upregulating Dll4/Notch signaling. *Dev Cell* 2010;**18**:938–949.
9. Schuijers J, Mokry M, Hatzis P, Cuppen E, Clevers H. Wnt-induced transcriptional activation is exclusively mediated by TCF/LEF. *EMBO J* 2014;**33**:146–156.
10. Yoon Y, Huang T, Tortelote GG, Wakamiya M, Hadjantonakis AK, Behringer RR, Rivera-Pérez JA. Extra-embryonic Wnt3 regulates the establishment of the primitive streak in mice. *Dev Biol* 2015;**403**:80–88.
11. Park C, Kim TM, Malik AB. Transcriptional regulation of endothelial cell and vascular development. *Circ Res* 2013;**112**:1380–1400.
12. Fish JE, Wythe JD. The molecular regulation of arteriovenous specification and maintenance. *Dev Dyn* 2015;**244**:391–409.
13. Sciorra VA, Morris AJ. Sequential actions of phospholipase D and phosphatidic acid phosphohydrolase 2b generate diglyceride in mammalian cells. *Mol Biol Cell* 1999;**10**:3863–3876.
14. Burnett C, Howard K. Fly and mammalian lipid phosphate phosphatase isoforms differ in activity both *in vitro* and *in vivo*. *EMBO Rep* 2003;**4**:793–799.
15. Brindley DN, Pilquil C. Lipid phosphate phosphatases and signaling. *J Lipid Res* 2009;**50**(Suppl.):S225–S230.
16. Tanyi JL, Hasegawa Y, Lapushin R, Morris AJ, Wolf JK, Berchuck A, Lu K, Smith DI, Kalli K, Hartmann LC, McCune K, Fishman D, Broaddus R, Cheng KW, Atkinson EN, Yamal JM, Bast RC, Felix EA, Newman RA, Mills GB. Role of decreased levels of lipid phosphate phosphatase-1 in accumulation of lysophosphatidic acid in ovarian cancer. *Clin Cancer Res* 2003;**9**:3534–3545.
17. Tanyi JL, Morris AJ, Wolf JK, Fang X, Hasegawa Y, Lapushin R, Auersperg N, Sigal YJ, Newman RA, Felix EA, Atkinson EN, Mills GB. The human lipid phosphate phosphatase-3 decreases the growth, survival, and tumorigenesis of ovarian cancer cells: validation of the lysophosphatidic acid signaling cascade as a target for therapy in ovarian cancer. *Cancer Res* 2003;**63**:1073–1082.
18. Yukiura H, Kano K, Kise R, Inoue A, Aoki J. LPP3 localizes LPA6 signalling to non-contact site in endothelial cells. *J Cell Sci* 2015;**128**:3871–3877.
19. Humtsoe JO, Feng S, Thakker GD, Yang J, Hong J, Wary KK. Regulation of cell-cell interactions by phosphatidic acid phosphatase 2b/VCIP. *EMBO J* 2003;**22**:1539–1554.
20. Wary KK, Thakker GD, Humtsoe JO, Yang J. Analysis of VEGF-responsive genes involved in the activation of endothelial cells. *Mol Cancer* 2003;**2**:25.
21. Wary KK, Humtsoe JO. Anti-lipid phosphate phosphohydrolase-3 (LPP3) antibody inhibits bFGF- and VEGF-induced capillary morphogenesis of endothelial cells. *Cell Commun Signal* 2005;**3**:9.

22. Humtsoe JO, Liu M, Malik AB, Wary KK. Lipid phosphate phosphatase 3 stabilization of beta-catenin induces endothelial cell migration and formation of branching point structures. *Mol Cell Biol* 2010;**30**:1593–1606.
23. Blais JD, Addison CL, Edge R, Falls T, Zhao H, Wary K, Koumenis C, Harding HP, Ron D, Holcik M, Bell JC. Perk-dependent translational regulation promotes tumor cell adaptation and angiogenesis in response to hypoxic stress. *Mol Cell Biol* 2006;**26**: 9517–9532.
24. Escalante-Alcalde D, Hernandez L, Le Stunff H, Maeda R, Lee HS, Cheng G Jr, Sciorra VA, Daar I, Spiegel S, Morris AJ, Stewart CL. The lipid phosphatase LPP3 regulates extra-embryonic vasculogenesis and axis patterning. *Development* 2003;**130**: 4623–4637.
25. Bréart B, Ramos-Perez WD, Mendoza A, Salous AK, Gobert M, Huang Y, Adams RH, Lafaille JJ, Escalante-Alcalde D, Morris AJ, Schwab SR. Lipid phosphate phosphatase 3 enables efficient thymic egress. *J Exp Med* 2011;**208**:1267–1278.
26. Panchatcharam M, Miriyala S, Salous A, Wheeler J, Dong A, Mueller P, Sunkara M, Escalante-Alcalde D, Morris AJ, Smyth SS. Lipid phosphate phosphatase 3 negatively regulates smooth muscle cell phenotypic modulation to limit intimal hyperplasia. *ATVB* 2013;**33**:52–59.
27. Panchatcharam M, Salous AK, Brandon J, Miriyala S, Wheeler J, Patil P, Sunkara M, Morris AJ, Escalante-Alcalde D, Smyth SS. Mice with targeted inactivation of ppap2b in endothelial and hematopoietic cells display enhanced vascular inflammation and permeability. *ATVB* 2014;**34**:837–845.
28. Koni PA, Joshi SK, Temann UA, Olson D, Burkly L, Flavell RA. Conditional vascular cell adhesion molecule 1 deletion in mice: impaired lymphocyte migration to bone marrow. *J Exp Med* 2001;**193**:741–754.
29. Kranz A, Fu J, Duerschke K, Weidlich S, Naumann R, Stewart AF, Anastassiadis K. An improved Flp deleter mouse in C57Bl/6 based on Flpo recombinase. *Genesis* 2010;**48**: 512–520.
30. Wary KK, Vogel SM, Garrean S, Zhao YD, Malik AB. Requirement of alpha(4)beta(1) and alpha(5)beta(1) integrin expression in bone-marrow-derived progenitor cells in preventing endotoxin-induced lung vascular injury and edema in mice. *Stem Cells* 2009;**27**:3112–3120.
31. Kohler EE, Wary KK, Li F, Chatterjee I, Urao N, Toth PT, Ushio-Fukai M, Rehman J, Park C, Malik AB. Flk1+ and VE-cadherin+ endothelial cells derived from iPSCs recapitulates vascular development during differentiation and display similar angiogenic potential as ESC-derived cells. *PLoS One* 2013;**8**:e85549.
32. Chatterjee I, Li F, Kohler EE, Rehman J, Malik AB, Wary KK. Induced pluripotent stem (iPS) cell culture methods and induction of differentiation into endothelial cells. *Methods Mol Biol* 2016;**1357**:311–327.
33. Nagy A, Gertsenstein M, Vintersten K, Behringer R. *Manipulating the Mouse Embryo, A Laboratory Manual*. 3rd ed. Cold Spring Harbor, NY: Cold Spring Harbor Laboratory Press; 2003.
34. Papaioannou VE, Behringer RR. Early embryonic lethality in genetically engineered mice: diagnosis and phenotypic analysis. *Vet Pathol* 2012;**49**:64–70.
35. Griffin CT, Curtis CD, Davis RB, Muthukumar V, Magnuson T. The chromatin-remodeling enzyme BRG1 modulates vascular Wnt signaling at two levels. *Proc Natl Acad Sci USA* 2011;**108**:2282–2287.
36. Skelly CL, Chandiwal A, Vosicky JE, Weichselbaum RR, Roizman B. Attenuated herpes simplex virus 1 blocks arterial apoptosis and intimal hyperplasia induced by balloon angioplasty and reduced blood flow. *Proc Natl Acad Sci USA* 2007;**104**:12474–12478.
37. Minami T, Yano K, Miura M, Kobayashi M, Suehiro J, Reid PC, Hamakubo T, Ryeom S, Aird WC, Kodama T. The Down syndrome critical region gene 1 short variant promoters direct vascular bed-specific gene expression during inflammation in mice. *J Clin Invest* 2009;**119**:2257–2270.
38. Tiruppathi C, Malik AB, Del Vecchio PJ, Keese CR, Giaever I. Electrical method for detection of endothelial cell shape change in real time: assessment of endothelial barrier function. *Proc Natl Acad Sci USA* 1992;**89**:7919–7923.
39. Cowan CE, Kohler EE, Dugan TA, Mirza MK, Malik AB, Wary KK. Kruppel-like factor-4 transcriptionally regulates VE-cadherin expression and endothelial barrier function. *Circ Res* 2010;**107**:959–966.
40. Schnürch H, Risau W. Expression of tie-2, a member of a novel family of receptor tyrosine kinases, in the endothelial cell lineage. *Development* 1993;**119**:957–968.
41. Maisonpierre PC, Suri C, Jones PF, Bartunkova S, Wiegand SJ, Radziejewski C, Compton D, McClain J, Aldrich TH, Papadopoulos N, Daly TJ, Davis S, Sato TN, Yancopoulos GD. Angiopoietin-2, a natural antagonist for Tie2 that disrupts in vivo angiogenesis. *Science* 1997;**277**:55–60.
42. Kisanuki YY, Hammer RE, Miyazaki J, Williams SC, Richardson JA, Yanagisawa M. Tie2-Cre transgenic mice: a new model for endothelial cell-lineage analysis in vivo. *Dev Biol* 2001;**230**:230–242.
43. Wary KK, Mainiero F, Isakoff SJ, Marcantonio EE, Giancotti FG. The adaptor protein Shc couples a class of integrins to the control of cell cycle progression. *Cell* 1996;**87**: 733–743.
44. Abdel-Latif A, Heron PM, Morris AJ, Smyth SS. Lysophospholipids in coronary artery and chronic ischemic heart disease. *Curr Opin Lipidol* 2015;**26**:432–437.
45. Wu C, Huang RT, Kuo CH, Kumar S, Kim CW, Lin YC, Chen YJ, Birukova A, Birukov KG, Dulin NO, Civelek M, Lusis AJ, Loyer X, Tedgui A, Dai G, Jo H, Fang Y. Mechanosensitive PPAP2B regulates endothelial responses to atherorelevant hemodynamic forces. *Circ Res* 2015;**117**:e41–e53.
46. de Lange FJ, Moorman AFM, Anderson RH, Manner J, Soufan AT, deGier-deVries C, Schneider MD, Webb S, Van Den Hoff MJ, Christoffels VM. Lineage and morphogenetic analysis of the cardiac valves. *Circ Res* 2004;**95**:645–654.
47. Armstrong EJ, Bischoff J. Heart valve development: endothelial cell signaling and differentiation. *Circ Res* 2004;**95**:459–470.
48. Yang JT, Rayburn H, Hynes RO. Cell adhesion events mediated by alpha 4 integrins are essential in placental and cardiac development. *Development* 1995;**121**:549–560.
49. Gaengel K, Niaudet C, Hagikura K, Laviña B, Muhl L, Hofmann JJ, Ebarasi L, Nyström S, Rymo S, Chen LL, Pang MF, Jin Y, Raschperger E, Roswall P, Schulte D, Benedito R, Larsson J, Hellström M, Fuxe J, Uhlén P, Adams R, Jakobsson L, Majumdar A, Vestweber D, Uv A, Betsholtz C. The sphingosine-1-phosphate receptor S1PR1 restricts sprouting angiogenesis by regulating the interplay between VE-cadherin and VEGFR2. *Dev Cell* 2012;**23**:587–599.
50. Ben Shoham A, Malkinson G, Krief S, Shwartz Y, Ely Y, Ferrara N, Yaniv K, Zelzer E. S1P1 inhibits sprouting angiogenesis during vascular development. *Development* 2012; **139**:3859–3869.
51. Schunkert H, König IR, Kathiresan S, Reilly MP, Assimes TL, Holm H, Preuss M, Stewart AF, Barbalic M, Gieger C, Absher D, Aherrahrou Z, Allayee H, Altshuler D, Anand SS, Andersen K, Anderson JL, Ardissino D, Ball SG, Balmforth AJ, Barnes TA, Becker DM, Becker LC, Berger K, Bis JC, Boekholdt SM, Boerwinkle E, Braund PS, Brown MJ, Burnett MS, Buysschaert I; Cardiogenics, Carlquist JF, Chen L, Cichon S, Codd V, Davies RW, Dedoussis G, Dehghan A, Demissie S, Devaney JM, Diemert P, Do R, Doering A, Eifert S, Mokhtari NE, Ellis SG, Elosua R, Engert JC, Epstein SE, de Faire U, Fischer M, Folsom AR, Freyer J, Gigante B, Girelli D, Gretarsdottir S, Gudnason V, Gulcher JR, Halperin E, Hammond N, Hazen SL, Hofman A, Horne BD, Illig T, Iribarren C, Jones GT, Jukema JW, Kaiser MA, Kaplan LM, Kastelein JJ, Khaw KT, Knowles JW, Kolovou G, Kong A, Laaksonen R, Lambrechts D, Leander K, Lettre G, Li M, Lieb W, Loley C, Lotery AJ, Mannucci PM, Maouche S, Martinelli N, McKeown PP, Meisinger C, Meitinger T, Melander O, Merlini PA, Mooser V, Morgan T, Mühleisen TW, Muhlestein JB, Münzel T, Musunuru K, Nahrstaedt J, Nelson CP, Nöthen MM, Olivieri O, Patel RS, Patterson CC, Peters A, Peyvandi F, Qu L, Quyyumi AA, Rader DJ, Rallidis LS, Rice C, Rosendaal FR, Rubin D, Salomaa V, Sampietro ML, Sandhu MS, Schadt E, Schäfer A, Schillert A, Schreiber S, Schrezenmeir J, Schwartz SM, Siscovick DS, Sivananthan M, Sivapalaratnam S, Smith A, Smith TB, Snoep JD, Soranzo N, Spertus JA, Stark K, Stirrups K, Stoll M, Tang WH, Tennstedt S, Thorgeirsson G, Thorleifsson G, Tomaszewski M, Uitterlinden AG, van Rij AM, Voight BF, Wareham NJ, Wells GA, Wichmann HE, Wild PS, Willenborg C, Witteman JC, Wright BJ, Ye S, Zeller T, Ziegler A, Cambien F, Goodall AH, Cupples LA, Quertermous T, März W, Hengstenberg C, Blankenberg S, Ouwehand WH, Hall AS, Deloukas P, Thompson JR, Stefansson K, Roberts R, Thorsteinsdottir U, O'Donnell CJ, McPherson R, Erdmann J. Large-scale association analyses identifies 13 new susceptibility loci for coronary artery disease. *Nat Genet* 2011;**43**:333–338.
52. Deloukas P, Kanoni S, Willenborg C, Farrall M, Assimes TL, Thompson JR, Ingelsson E, Saleheen D, Erdmann J, Goldstein BA, Stirrups K, König IR, Cazier JB, Johansson A, Hall AS, Lee JY, Willer CJ, Chambers JC, Esko T, Folkersen L, Goel A, Grundberg E, Havulinna AS, Ho WK, Hopewell JC, Eriksson N, Kleber ME, Kristiansson K, Lundmark P, Lyytikäinen LP, Rafelt S, Shungin D, Strawbridge RJ, Thorleifsson G, Tikkanen E, Van Zuydam N, Voight BF, Waite LL, Zhang W, Ziegler A, Absher D, Altshuler D, Balmforth AJ, Barroso I, Braund PS, Burgdorf C, Claudi-Boehm S, Cox D, Dimitriou M, Do R; DIAGRAM Consortium; CARDIOGENICS Consortium, Doney AS, El Mokhtari N, Eriksson P, Fischer K, Fontanillas P, Franco-Cereceda A, Gigante B, Groop L, Gustafsson S, Hager J, Hallmans G, Han BG, Hunt SE, Kang HM, Illig T, Kessler T, Knowles JW, Kolovou G, Kuusisto J, Langenberg C, Langford C, Leander K, Lokki ML, Lundmark A, McCarthy MI, Meisinger C, Melander O, Mihailov E, Maouche S, Morris AD, Müller-Nurasyid M; MuTHER Consortium, Nikus K, Peden JF, Rayner NW, Rasheed A, Rosinger S, Rubin D, Rumpf MP, Schäfer A, Sivananthan M, Song C, Stewart AF, Tan ST, Thorgeirsson G, van der Schoot CE, Wagner PJ; Wellcome Trust Case Control Consortium, Wells GA, Wild PS, Yang TP, Amouyel P, Arveiler D, Basart H, Boehnke M, Boerwinkle E, Brambilla P, Cambien F, Cupples AL, de Faire U, Dehghan A, Diemert P, Epstein SE, Evans A, Ferrario MM, Ferrières J, Gauguier D, Go AS, Goodall AH, Gudnason V, Hazen SL, Holm H, Iribarren C, Jang Y, Kähönen M, Kee F, Kim HS, Klopp N, Koenig W, Kratzer W, Kuulasmaa K, Laakso M, Laaksonen R, Lee JY, Lind L, Ouwehand WH, Parish S, Park JE, Pedersen NL, Peters A, Quertermous T, Rader DJ, Salomaa V, Schadt E, Shah SH, Sinisalo J, Stark K, Stefansson K, Trégouët DA, Virtamo J, Wallentin L, Wareham N, Zimmermann ME, Nieminen MS, Hengstenberg C, Sandhu MS, Pastinen T, Syvänen AC, Hovingh GK, Dedoussis G, Franks PW, Lehtimäki T, Metspalu A, Zalloua PA, Siegbahn A, Schreiber S, Ripatti S, Blankenberg SS, Perola M, Clarke R, Boehm BO, O'Donnell C, Reilly MP, März W, Collins R, Kathiresan S, Hamsten A, Kooner JS, Thorsteinsdottir U, Danesh J, Palmer CN, Roberts R, Watkins H, Schunkert H, Samani NJ. Large-scale association analysis identifies new risk loci for coronary artery disease. CARDIoGRAMplusC4D Consortium. *Nat Genet* 2013;**45**:25–33.
53. Duan S, Luo X, Dong C. Identification of susceptibility modules for coronary artery disease using a genome wide integrated network analysis. *Gene* 2013;**531**:347–354.
54. Smyth SS, Mueller P, Yang F, Brandon JA, Morris AJ. Arguing the case for the autotaxin-lysophosphatidic acid-lipid phosphate phosphatase 3-signaling nexus in the development and complications of atherosclerosis. *ATVB* 2014;**34**:479–486.